University of Science and Technology of China
USTC Hefei, April 2023

F Hautmann

Factorization and Resummation Methods in Physics at High Energy Colliders

Thank you very much for this invitation – it is a great pleasure for me to visit USTC!

Collision Event at the Large Hadron Collider (LHC)

- Probe shortest distances by high momentum transfer scattering ("hard scattering")
- Radiative processes by strong interactions - initial-state and final-state QCD "parton showers"
- "Hadronization" over long time and distance scales
- Multiple parton interactions and soft particle production ("underlying event")

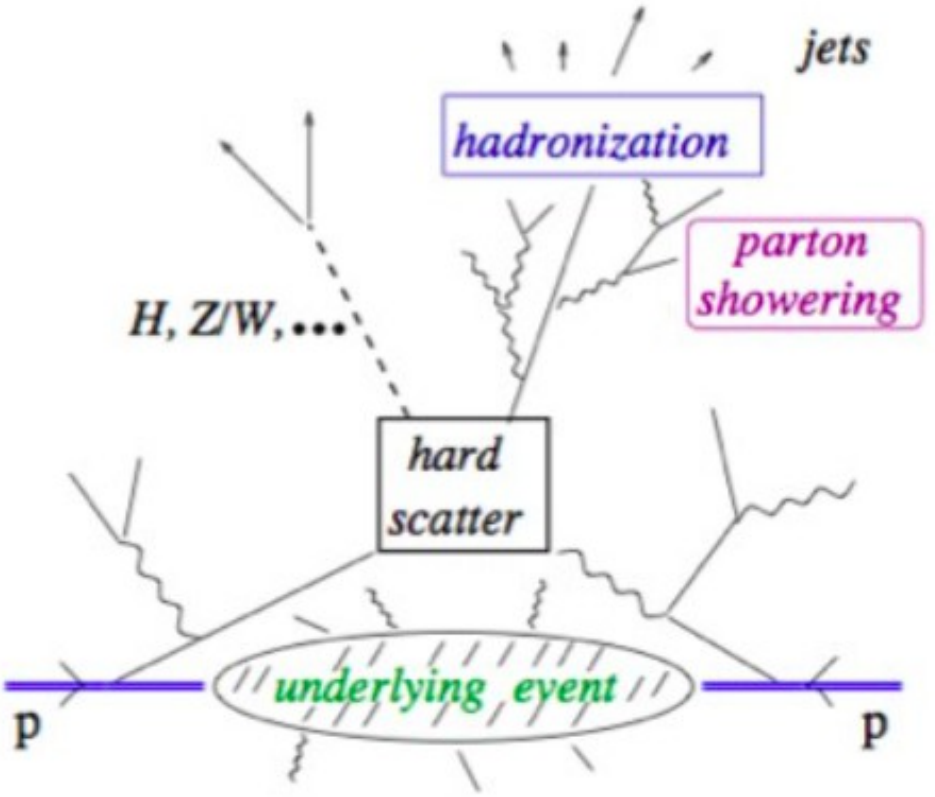

A cartoon picture of collider's phase space

- New physics probed at distances r ~ 1 / Q
  (Q = hard momentum scale)
- Collision energy $s^{1/2} \sim x^{-1} Q$

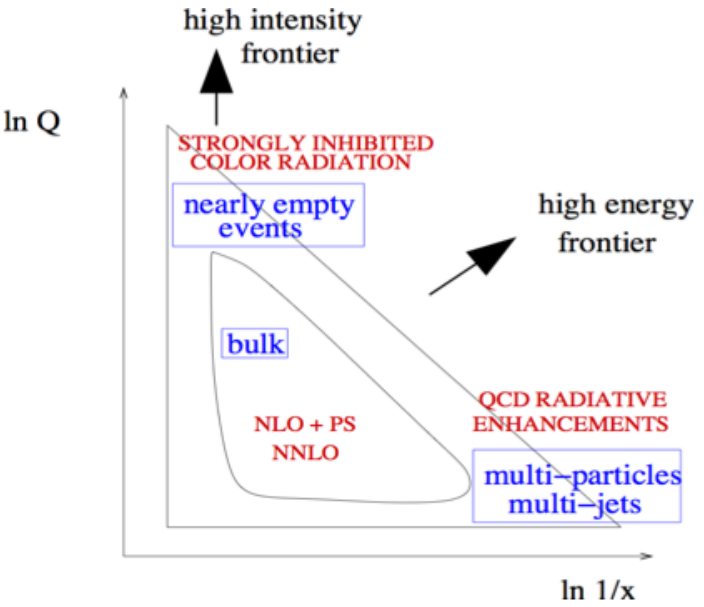

Phase space in high-energy hadron collisions

- *Bulk of phase space*
  treatable by methods employed routinely in collider physics: LO, NLO, or NNLO perturbation expansions, matched with "parton-shower" Monte Carlo algorithms
- *Extreme regions near phase space boundary*
  call for cutting-edge factorization and resummation methods which go beyond finite-order perturbation theory

Quantum Chromodynamics (QCD) at the "extremes"

Factorization theorems

- implement renormalization group (RG) evolution
- allow one to systematically take into account perturbative and nonperturbative contributions to high-energy cross sections
- Generalizations of RG factorization to multiple-scale problems are required to treat

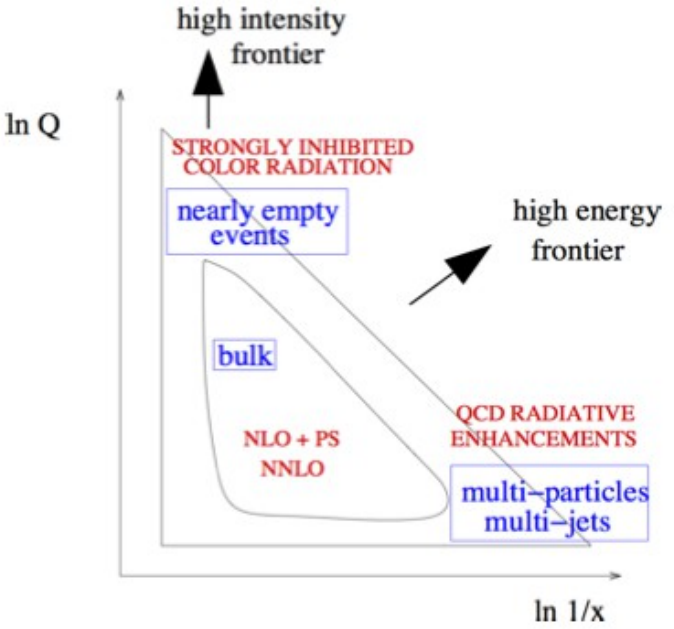

QCD at the "extremes":

- region of *enhanced* color radiation, where partons' longitudinal momenta are small or comparable to their transverse momentum components;
- region of *inhibited* color radiation, where partons' longitudinal momenta are large and approach their exclusive phase-space frontier.

Remark on QCD as a part of the Standard Model (SM) of Fundamental Interactions

- Quantum Chromodynamics (QCD), the gauge theory of the strong interaction, is the sector of the SM which is expected to exist as a fundamental theory down to arbitrarily short distances

- On one hand, one relies on QCD to search for new physics in the electroweak sector with high-energy experiments
- On the other hand, one investigates in QCD profound questions probing field theory in “extreme” regions

OUTLINE

- Principles of factorization and resummation
- Recent advances on precision electroweak boson physics at the LHC and TMD formalisms
- Impact on multi-jet final states associated to electroweak boson production

PRINCIPLES OF FACTORIZATION

A) $V \to$ hadrons

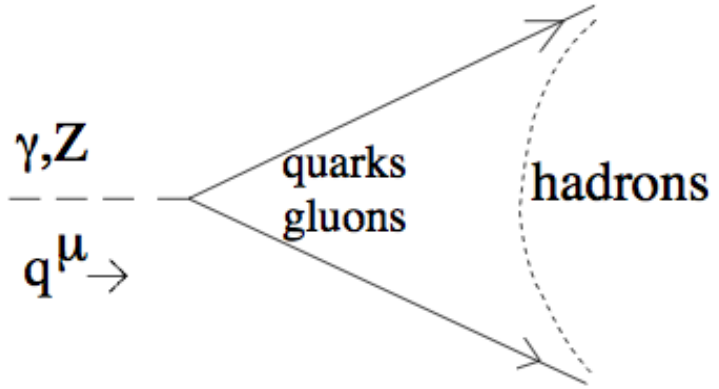

$\sqrt{Q^2} = \sqrt{q^\mu q_\mu} \gg$ "hadronic scale" $\approx \Lambda_{\rm QCD} \approx 1$ fermi $^{-1}$

- Separate short-time and long-time dynamics: $(\Delta t)_{partonic} \approx Q^{-1} \ll (\Delta t)_{hadroniz.} \approx \Lambda_{\rm QCD}^{-1}$

$$\Rightarrow \quad P(e^+e^- \to h) = P(e^+e^- \to q\bar{q})\, P(q\bar{q} \to h)$$

- Next use completeness : $\sum_h P(i \to h) = 1 \;\Rightarrow$

$$\Rightarrow \quad \sigma_{\rm tot}(e^+e^- \to h) \equiv \sum_h P(e^+e^- \to h)$$

$$= P(e^+e^- \to q\bar{q}) \sum_h P(q\bar{q} \to h) = P(e^+e^- \to q\bar{q})$$

▷ almost right — but not quite: rhs is IR-divergent in PT... ↪

↪ particle number nonconservation ⇒ add in multi-particle states

($q\bar{q}g$ to 1st order)

⇒ $\sigma(e^+e^-\to q\bar{q}) + \sigma(e^+e^-\to q\bar{q}g)$ insensitive to long-time interactions:

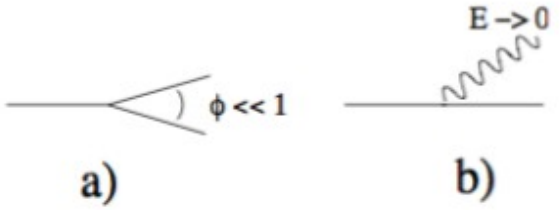

i.e., insensitive to collinear and soft parton emission

• perturbative calculability (= "IR-safety")

♠ valid to *any* order in α_s:

$$\sigma_{\rm tot}(e^+e^-\to h) = \sigma_0 \left[1 + \frac{\alpha_s}{\pi} + 1.4092\left(\frac{\alpha_s}{\pi}\right)^2 - 12.805\left(\frac{\alpha_s}{\pi}\right)^3 + \ldots\right]$$

♠ valid for large classes of *infrared-safe* observables:

▷ accurate determinations of QCD running coupling $\alpha_s(Q^2)$

THE QCD RUNNING COUPLING

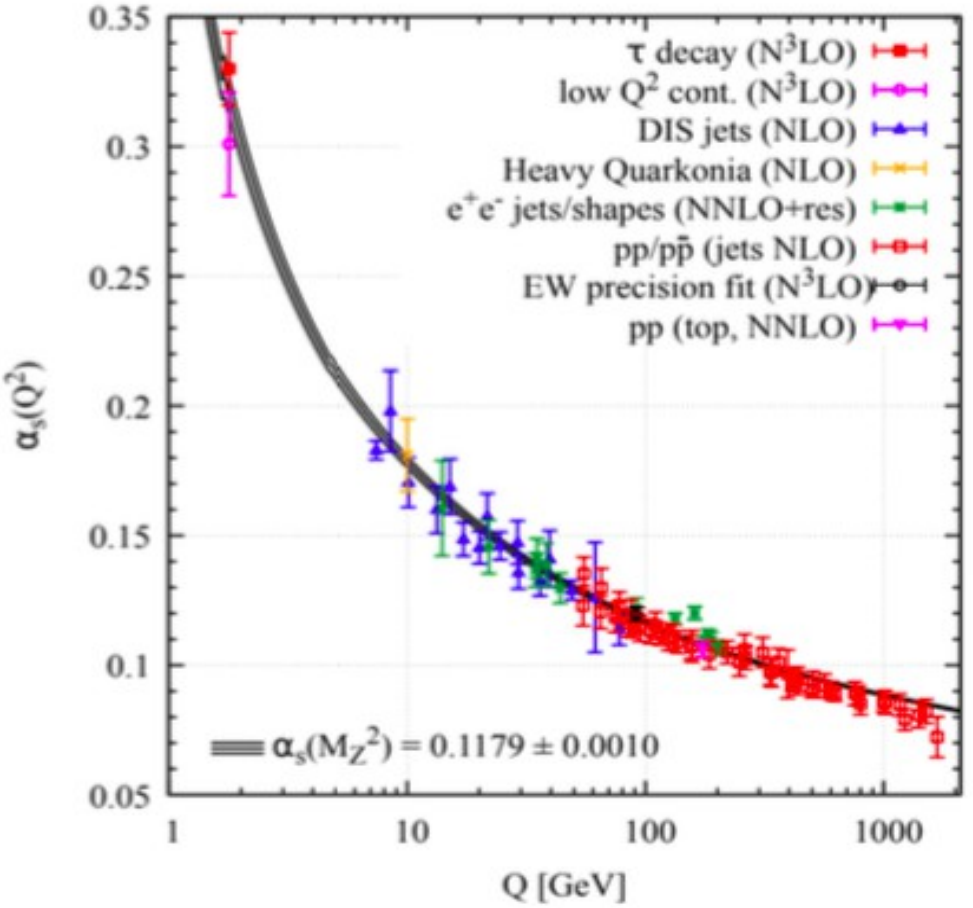

α_s extracted from measurements by using QCD perturbation theory. (Ref: Particle Data Group, Prog. Theor. Exp. Phys. 2020, 083C01 (2020))

B) Hadron scattering. E.g., DIS

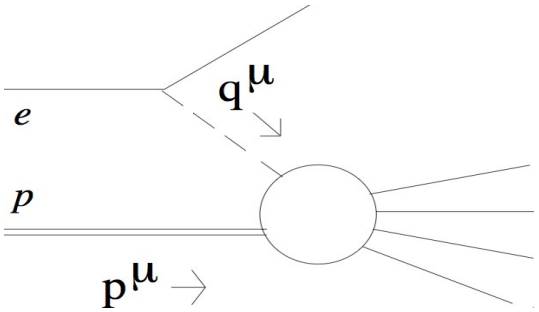

- necessarily sensitive to long timescales, BUT

$$\sigma(Q,m) = C(Q, \text{parton momenta } > \mu) \otimes f(\text{parton momenta } < \mu, m)$$

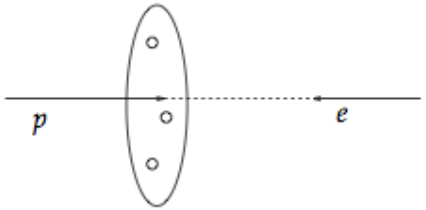

$\delta t_{\text{scatter}} \ll \tau_{\text{parton}}$ in "infinite-momentum" frame

The collinear parton density functions:

$$\text{Pdf's}: \quad f(x,\mu) = \int \frac{dy^-}{2\pi}\, e^{-ixp^+y^-}\, \tilde{f}(y)$$

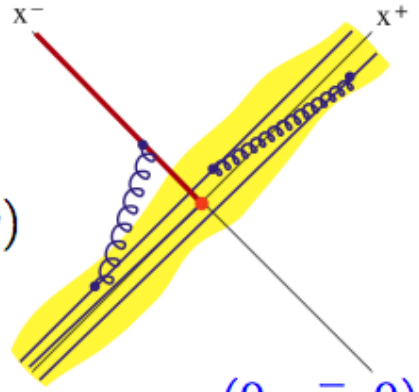

$$\tilde{f}(y) = \langle\, P \mid \overline{\psi}(y)\, V_y^\dagger(n)\, \gamma^+\, V_0(n)\, \psi(0) \mid P \,\rangle \quad , \qquad y = (0, y^-, 0)$$

$$V_y(n) = \mathcal{P} \exp\left(ig_s \int_0^\infty d\tau\; n \cdot A(y + \tau\, n)\right)$$

correlation of parton fields at lightcone distances

Hadron scattering. E.g.: DIS

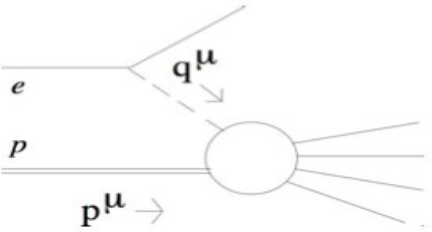

♢ Renormalization group invariance ⇒

$$\frac{d}{d\ln\mu}\,\sigma = 0 \quad \Rightarrow \quad \frac{d}{d\ln\mu}\,\ln f = \gamma = -\frac{d}{d\ln\mu}\,\ln C$$

↪ DGLAP evolution equations [Altarelli-Parisi Dokshitzer Gribov-Lipatov]

$$f = f_0 \times \exp\int \frac{d\mu}{\mu}\,\gamma(\alpha_s(\mu))$$

↗ resummation of $(\alpha_s \ln Q/\Lambda_{\rm QCD})^n$ to all orders in PT

Note: expansions $\gamma \simeq \gamma^{(LO)}\,(1 + b_1\alpha_s + b_2\alpha_s^2 + ...)$

$$C \simeq C^{(LO)}\left(1 + c_1\alpha_s + c_2\alpha_s^2 + ...\right)$$

give LO, NLO, NNLO, ... logarithmic corrections

PARTON DISTRIBUTION FUNCTIONS

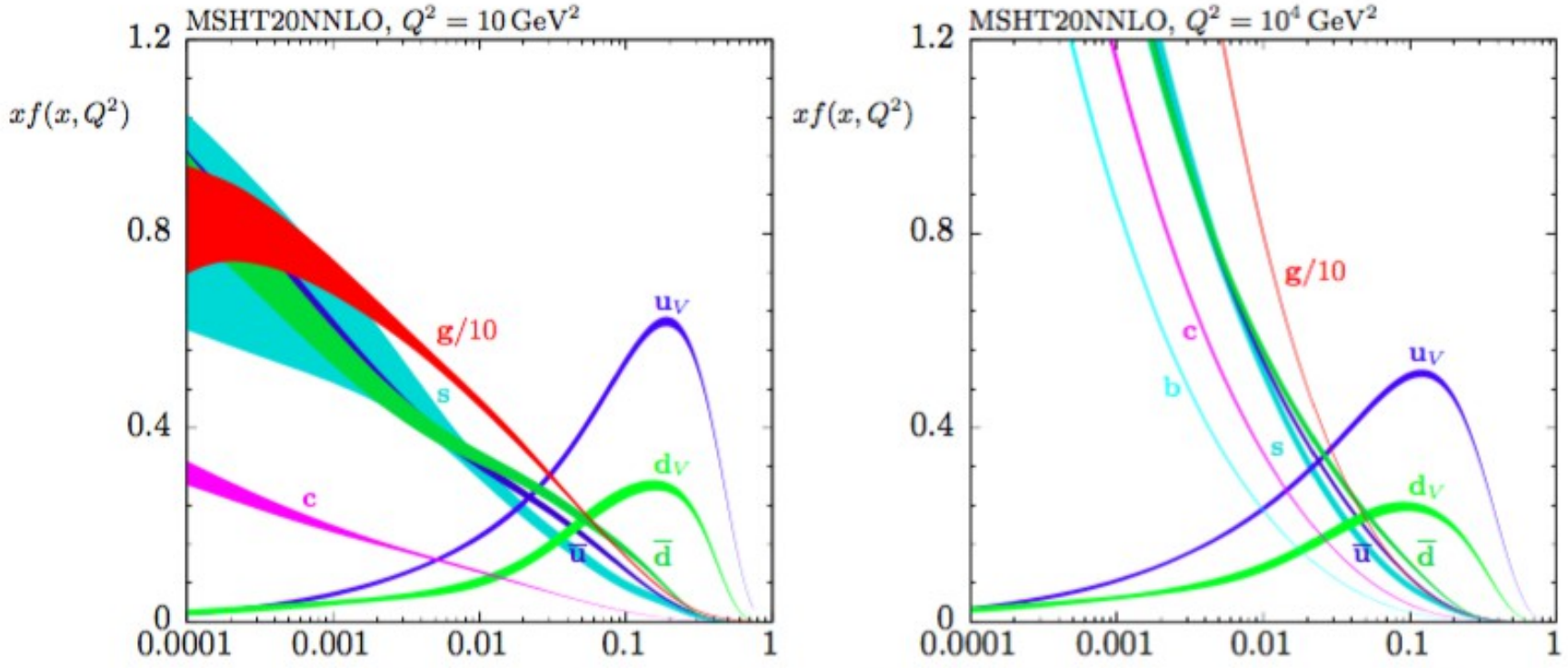

Figure 1: MSHT20 NNLO PDFs at $Q^2 = 10\ \mathrm{GeV}^2$ and $Q^2 = 10^4\ \mathrm{GeV}^2$, with associated 68% confidence-level uncertainty bands.

E. Phys. J. C81 (2021) 341

C) Multiple-scale hard scattering at high energies

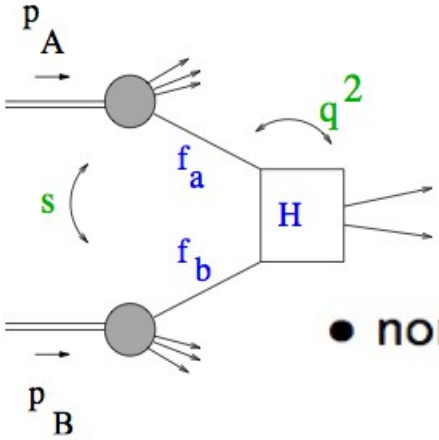

$$s \gg q_1^2 \gg \cdots q_n^2 \gg \Lambda^2_{\rm QCD}$$

- nonperturbative components probed near kinematic boundaries $(x \to 0,\ 1-x \to 0)$
- more complex, potentially large corrections to all orders in α_s, $\sim \ln^k(q_i^2/q_j^2)$

$$e.g.\ \ C \simeq C^{(LO)}\left(1 + c_1\alpha_s + \ldots + c_{n+m}\alpha_s^m(\alpha_s\ L)^n + \ldots\right)\ ,\ L = \text{“large log”}$$

$\hookrightarrow$ yet summable by QCD techniques that

▷ generalize RG factorization

▷ extend parton correlation functions off the lightcone

$\Rightarrow$ unintegrated (or TMD) pdf's

♠ new nonperturbative information; generalized evolution equations

TRANSVERSE MOMENTUM DEPENDENT (TMD) PARTON CORRELATION FUNCTIONS

- Correlation functions at non-lightlike distances:

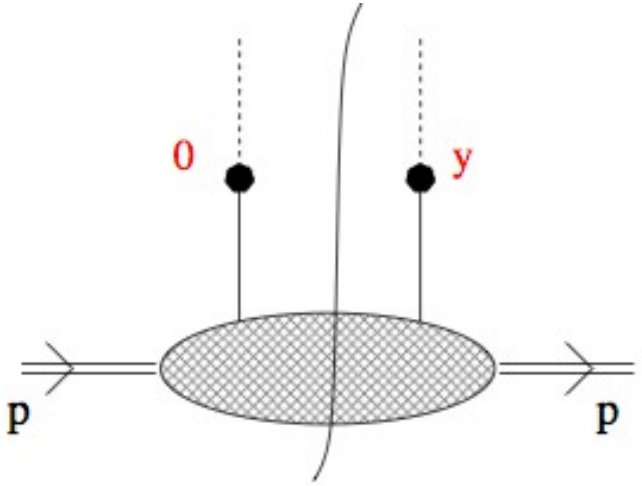

$$p = (p^+, m^2/2p^+, 0_\perp)$$

$$\tilde{f}(y) = \langle\, P \mid \overline{\psi}(y)\, V_y^\dagger(n)\, \gamma^+\, V_0(n)\, \psi(0) \mid P \,\rangle \quad , \qquad y = (0, y^-, y_\perp)$$

$$V_y(n) = \mathcal{P} \exp\left(i g_s \int_0^\infty d\tau\; n \cdot A(y + \tau\, n) \right)$$

- TMD pdfs:

$$f(x, k_\perp) = \int \frac{dy^-}{2\pi} \frac{d^{d-2} y_\perp}{(2\pi)^{d-2}} e^{-ixp^+ y^- + ik_\perp \cdot y_\perp} \tilde{f}(y)$$

TMD factorization and parton distribution functions

I) low q_T : $q_T \ll Q$

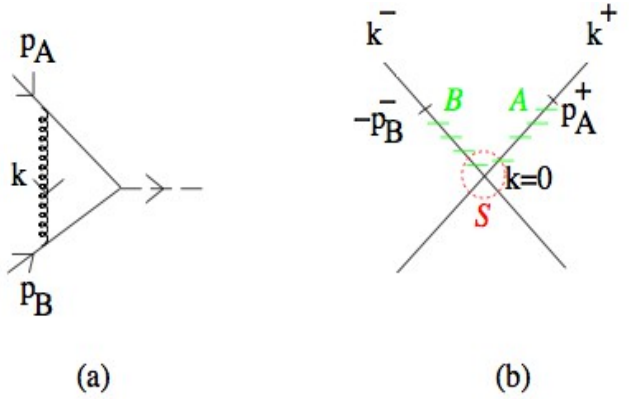

$\alpha_s^n \ln^m Q/q_T$

II) high $\sqrt{s}$: $\sqrt{s} \gg M$

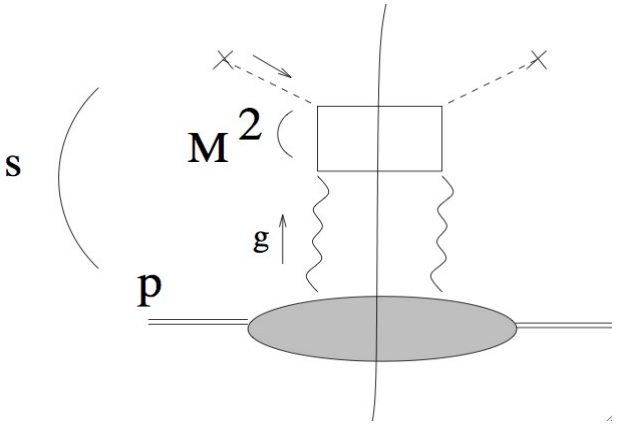

$(\alpha_s \ln \sqrt{s}/M)^n$

Low-qT factorization

(with CSS* evolution - or variants)

[*Collins-Soper-Sterman]

High-energy factorization

(with BFKL* evolution - or variants)

[*Balitsky-Fadin-Kuraev-Lipatov]

R. Angeles-Martinez et al., “Transverse momentum dependent (TMD) parton distribution functions: status and prospects”, Acta Phys. Polon. B46 (2015) 2501

PRECISION ELECTROWEAK BOSON PHYSICS AT THE LHC AND TMD FORMALISMS

p_T^Z Resummation Benchmarking
Status Report

Johannes Michel
MIT Center for Theoretical Physics

On behalf of the WG 1 Resummation Subgroup

LHC EW WG General Meeting
CERN and remote locations, February 17, 2022

slides by J. Michel (2022)

LHC Electroweak Working Group

Introduction

Why we're doing this …

- W mass measurements at the LHC use precisely measured p_T^Z (or ϕ_η^*) spectrum
- Theory input needed to relate p_T^Z and p_T^W
- Fixed-order predictions diverge for $p_T^Z \ll m_Z$ due to large Sudakov double logs
  - ► All-order resummation required to high (logarithmic) perturbative accuracy

Who is doing this …

- On the theory side, p_T^Z spectrum is of key interest to many different communities
  e.g. TMD/proton structure, resummation in direct QCD/SCET, fixed-order subtractions
- ► Many mature formalisms and codes to perform all-order resummation

Goal of the benchmarking effort

- Compare predictions & understand their differences, uncertainties, and accuracy

One theorist's implicit assumption is another theorist's uncertainty …

Resummation basics: Power expansion of the spectrum at small p_T

Structure of the fixed-order spectrum for $p_T \ll Q \equiv \sqrt{q^2} = m_{\ell\ell}$:

$$\frac{\mathrm{d}\sigma}{\mathrm{d}p_T} = \delta(p_T) + \alpha_s\left[\frac{L}{p_T} + \frac{1}{p_T} + \delta(p_T) + f_1^{\text{nons}}(p_T)\right] + \alpha_s^2\left[\frac{L^3}{p_T} + \frac{L^2}{p_T} + \frac{L}{p_T} + \frac{1}{p_T} + \delta(p_T) + f_2^{\text{nons}}(p_T)\right] + \vdots \quad \vdots \quad \vdots \quad \vdots \quad \ddots + \dots \Big]$$

$$\sim (1/p_T)\left[\mathcal{O}(1) + \mathcal{O}(p_T^2/Q^2)\right]$$

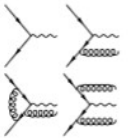

- "Singular" or "leading power" terms
  - Large logarithms $L \equiv \ln p_T/Q$ left after real/virtual IR poles cancel
  - To be resummed to all orders
- "Nonsingular" or "subleading power"
  - Suppressed by relative p_T^2/Q^2
    [for incl. Z – see talk by L. Buonocore for fiducial!]
  - Supplied by matching to full FO

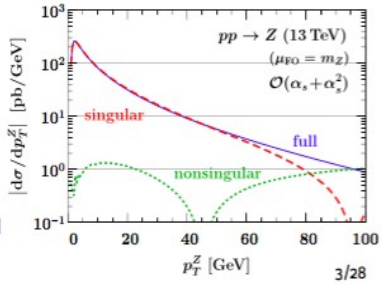

3/28

TMD formalism for Drell-Yan (DY) electroweak boson production

- Low-qT factorization/evolution

We start from the TMD factorization formula for the differential cross section for DY lepton pair production $h_1 + h_2 \to Z/\gamma^*(\to ll') + X$ at low $q_T \ll Q$ [13]

$$\frac{d\sigma}{dQ^2 dy dq_T^2} = \sigma_0 \sum_{f_1,f_2} H_{f_1 f_2}(Q,\mu) \int \frac{d^2\boldsymbol{b}}{4\pi} e^{i\boldsymbol{b}\cdot\boldsymbol{q}_T} F_{f_1\leftarrow h_1}(x_1,\boldsymbol{b};\mu,\zeta_1) F_{f_2\leftarrow h_2}(x_2,\boldsymbol{b};\mu,\zeta_2) + O(q_T/Q) + O(\Lambda_{\rm QCD}/Q), \quad (1)$$

where Q^2, $\boldsymbol{q}_T$ and y are the invariant mass, transverse momentum and rapidity of the lepton pair, and the TMD distributions $F_{f\leftarrow h}$ fulfill evolution equations in rapidity

$$\frac{\partial \ln F_{f\leftarrow h}}{\partial \ln \zeta} = -\mathcal{D}^f(\mu,\boldsymbol{b}) \quad (2)$$

rapidity evolution (Collins-Soper kernel)

and in mass

$$\frac{\partial \ln F_{f\leftarrow h}}{\partial \ln \mu} = \gamma_F(\alpha_s(\mu),\zeta/\mu^2) \ , \qquad \frac{\partial \mathcal{D}^f(\mu,\boldsymbol{b})}{\partial \ln \mu} = \frac{1}{2}\Gamma_{\rm cusp}(\alpha_s(\mu)) \ . \quad (3)$$

renormalization group evolution

cusp anomalous dimension

- Small-b expansion

We further perform the small-$\boldsymbol{b}$ operator product expansion of the TMD $F_{f\leftarrow h}$ as follows,

$$F_{f\to h}(x,\boldsymbol{b}) = f_{\rm NP}(x,\boldsymbol{b}) \sum_{f'} \int_x^1 \frac{dy}{y} C_{f\leftarrow f'}\left(\frac{x}{y}, \ln\left(\boldsymbol{b}^2\mu^2\right)\right) f_{f'\leftarrow h}(y,\mu), \quad (4)$$

OPE

where $f_{f'\leftarrow h}$ are the PDFs, $C_{f\leftarrow f'}$ are the matching Wilson coefficients, and $f_{\rm NP}$ are functions[1] to be fitted to data.

Perturbative resummation

– The summation of logarithmically-enhanced corrections at low qT is achieved by computing perturbatively the functions H, C, gamma and Gamma as series expansions in powers of alpha_s

- Ex.: next-to-next-to-leading-logarithmic (N2LL) accuracy

H	$C_{f\leftarrow f'}$	Γ_{cusp}	γ_F	α_s running	PDF evolution
α_s^2	α_s^2	α_s^3	α_s^3	NNLO	

- Recent N3LL (and beyond) - e.g., *Ebert et al, JHEP 09 (2020) 146; Luo et al, PRL 124 (2020) 092001; Chen et al, PRL 124 (2022) 252001; Neumann et al, PRD 107 (2023) 011506*

Non-perturbative contributions

-- intrinsic kT distributions enter as boundary conditions to mass evolution equations for TMDs

– nonperturbative Sudakov effects enter through kernel of rapidity evolution equations for TMDs

- Recent studies from fits of theory to experiment: *Bury et al, JHEP 10 (2022) 118; Bacchetta et al, JHEP 10 (2022) 127*

RECENT DETERMINATIONS OF RAPIDITY EVOLUTION KERNEL *D (b, mu)*

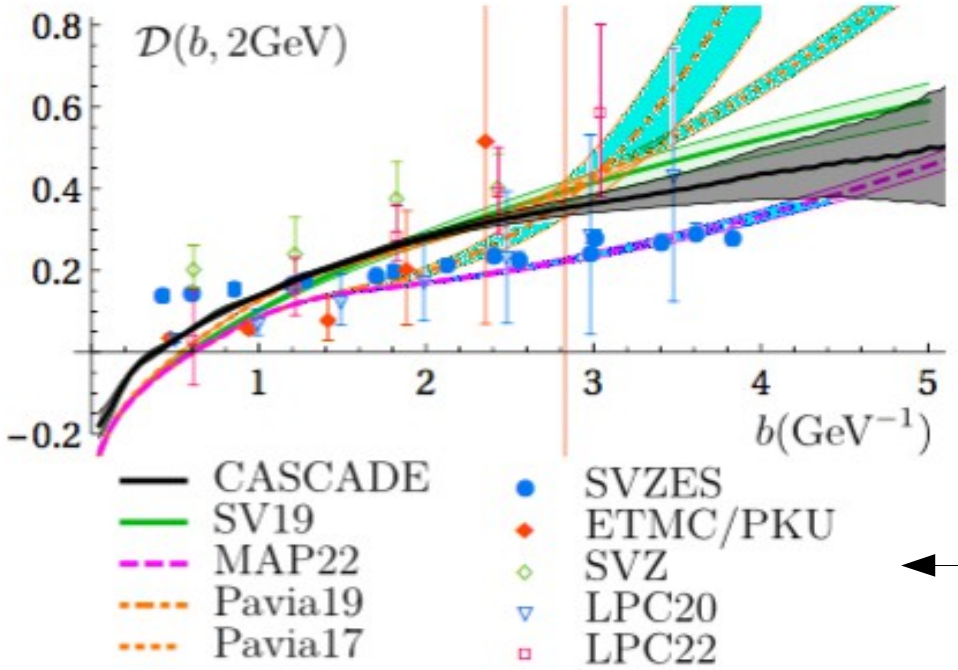

A Bermudez Martinez and A Vladimirov, Phys. Rev. D 106 (2022) L091501 [arXiv:2206.01105]

Determinations of kernel *D* from different approaches:
- fits to experimental data;
- lattice calculations;
- TMD Monte Carlo calculations.

NB: determinations of *D* from data fits in this figure assume either quadratic (a la Resbos) or linear behavior in *b* at large *b.* The alternative possibility of constant behavior at large *b* is studied in arXiv:2002.12810, arXiv:2109.12051 (similar in spirit to 's-channel picture' [Soper & H, PRD 75 (2007) 074020]).

- Next we concentrate on studies (based on arXiv:2201.07114) to assess TMD uncertainties in current extractions from fits to experimental data.

TMD EXTRACTION FROM DY EXPERIMENTAL DATA: inclusion of PDF uncertainty and flavor dependence

[Bury, Leal Gomez, Scimemi, Vladimirov, Zurita & H, JHEP 10 (2022) 118 [arXiv:2201.07114]]

- TMD-factorized DY formula implemented in `artemide` at NNLL';
  collinear sets from `LHAPDF`;
  minimization by `iMinuit`.

- Represent PDF as MC ensemble
- Uncertainties by fitting each member of input ensemble
- Two uncertainty sources, EXP and PDF

$$\delta \equiv \frac{\langle q_T \rangle}{\langle Q \rangle} < 0.1, \quad \text{or} \quad \delta < 0.25 \quad \text{if} \quad \delta^2 < \sigma$$

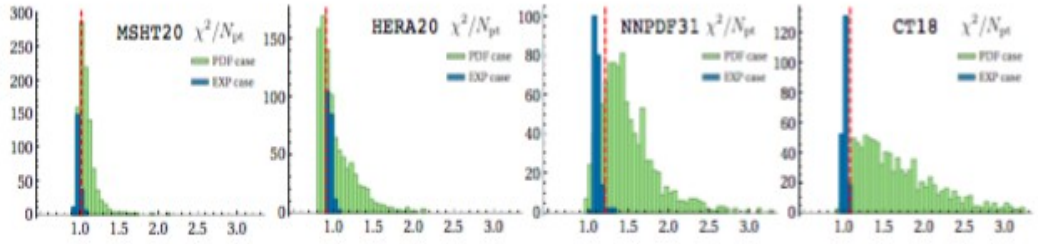

Figure 5: Distribution of χ^2-values for the **PDF** and **EXP** cases. The red lines show the position of the final χ^2-value.

		MSHT20	HERA20	NNPDF31	CT18
Data set	N_{pt}	χ^2/N_{pt}	χ^2/N_{pt}	χ^2/N_{pt}	χ^2/N_{pt}
CDF run1	33	0.78	0.61	0.72	0.75
CDF run2	39	1.70	1.42	1.68	1.79
D0 run1	16	0.71	0.81	0.79	0.79
D0 run2	8	1.95	1.39	1.92	2.00
D0 run2 (μ)	3	0.50	0.59	0.55	0.52
ATLAS 7TeV 0.0<|y|<1.0	5	4.06	1.94	2.12	4.21
ATLAS 7TeV 1.0<|y|<2.0	5	7.78	4.83	4.52	6.12
ATLAS 7TeV 2.0<|y|<2.4	5	2.57	2.18	3.65	2.39
ATLAS 8TeV 0.0<|y|<0.4	5	2.98	3.66	2.12	3.23
ATLAS 8TeV 0.4<|y|<0.8	5	2.00	1.53	4.52	3.21
ATLAS 8TeV 0.8<|y|<1.2	5	1.00	0.50	2.75	1.89
ATLAS 8TeV 1.2<|y|<1.6	5	2.25	1.61	2.49	2.72
ATLAS 8TeV 1.6<|y|<2.0	5	1.92	1.68	2.86	1.96
ATLAS 8TeV 2.0<|y|<2.4	5	1.35	1.14	1.47	1.06
ATLAS 8TeV 46<Q<66GeV	3	0.59	1.86	0.23	0.05
ATLAS 8TeV 116<Q<150GeV	7	0.61	1.03	0.85	0.70
CMS 7TeV	8	1.22	1.19	1.30	1.25
CMS 8TeV	8	0.78	0.77	0.75	0.78
CMS 13TeV 0.0<|y|<0.4	8	3.52	1.93	2.13	3.73
CMS 13TeV 0.4<|y|<0.8	8	1.06	0.53	0.71	1.65
CMS 13TeV 0.8<|y|<1.2	10	0.48	0.14	0.33	0.88
CMS 13TeV 1.2<|y|<1.6	11	0.62	0.33	0.47	0.86
CMS 13TeV 1.6<|y|<2.4	13	0.46	0.32	0.39	0.57
LHCb 7TeV	8	1.79	1.00	1.62	1.16
LHCb 8TeV	7	1.38	1.29	1.63	0.83
LHCb 13TeV	9	1.28	0.84	1.07	0.93
PHE200	3	0.29	0.42	0.38	0.29
E228-200	43	0.43	0.36	0.57	0.43
E228-300 Q < 9GeV	43	0.77	0.56	0.89	0.55
E228-300 Q > 11GeV	10	0.29	0.37	0.45	0.44
E228-400 Q < 9GeV	34	2.19	1.15	1.49	1.34
E228-400 Q > 11GeV	42	0.25	0.61	0.44	0.40
E772	35	1.14	1.37	1.79	1.11
E605 Q < 9GeV	21	0.52	0.47	0.47	0.61
E605 Q > 11GeV	32	0.47	0.73	1.34	0.52
Total	**507**	**1.12**	**0.91**	**1.21**	**1.08**

Table 3: Distribution of the values of χ^2 over the TMD data set in fits with different PDF input.

Description of High-Energy and Low-Energy Data by TMDs with EXP and PDF Uncertainties

[Bury, Leal Gomez, Scimemi, Vladimirov, Zurita & H, JHEP 10 (2022) 118 [arXiv:2201.07114]]

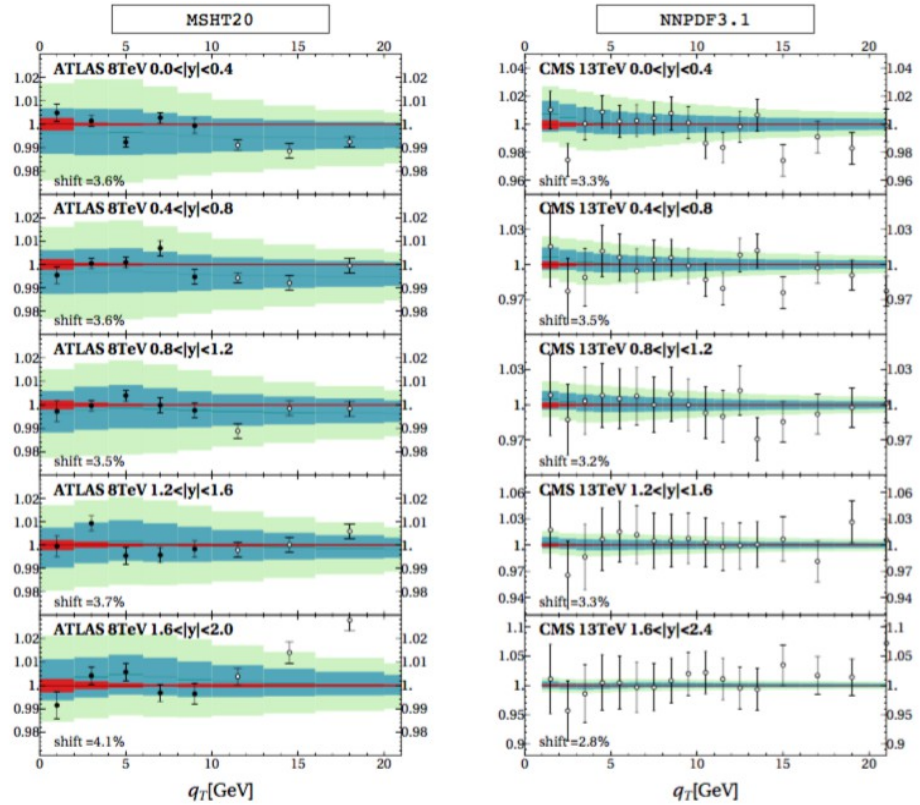

Figure 3: Example of the data description at high energy. Left panel: the ratio $d\sigma_{\text{experiment}}/d\sigma_{\text{theory}}$ for Z-boson production at 8 TeV measured by the ATLAS experiment with MSHT20. Right panel: the ratio $d\sigma_{\text{experiment}}/d\sigma_{\text{theory}}$ for Z-boson production at 13 TeV at the CMS experiment with NNPDF3.1. The red band is the **EXP**-uncertainty. The light-green band is the **PDF**-uncertainty. The blue band is the combined uncertainty. Only the filled bullets are included into the fit.

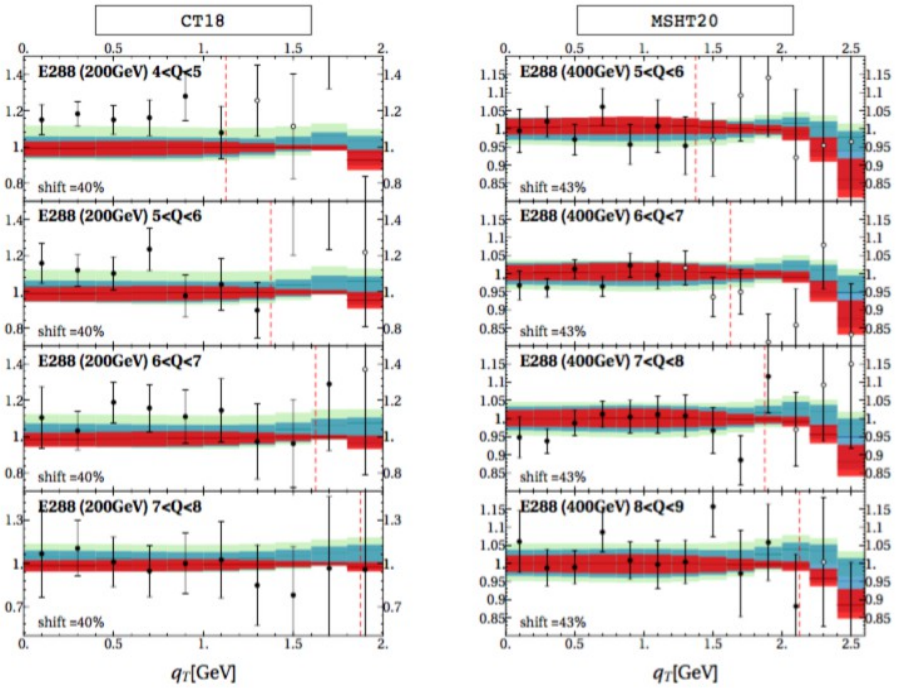

Figure 4: Example of the data description at low energy. Left panel: ratio $d\sigma_{\text{experiment}}/d\sigma_{\text{theory}}$ for the DY process at E288 experiment with 200 GeV beam-energy with CT18. Right panel: ratio $d\sigma_{\text{experiment}}/d\sigma_{\text{theory}}$ for the DY process at E288 experiment with 400 GeV beam-energy with MSHT20. Red band is the **EXP**-uncertainty. Light-green band is the **PDF**-uncertainty. The blue band is the combined uncertainty. The filled bullets are included into the fit. The dashed red vertical lines illustrate the cut $q_T < 0.25Q$ discussed at the beginning of sec. 3.

Flavour dependence of the TMDs

flavor-independent case

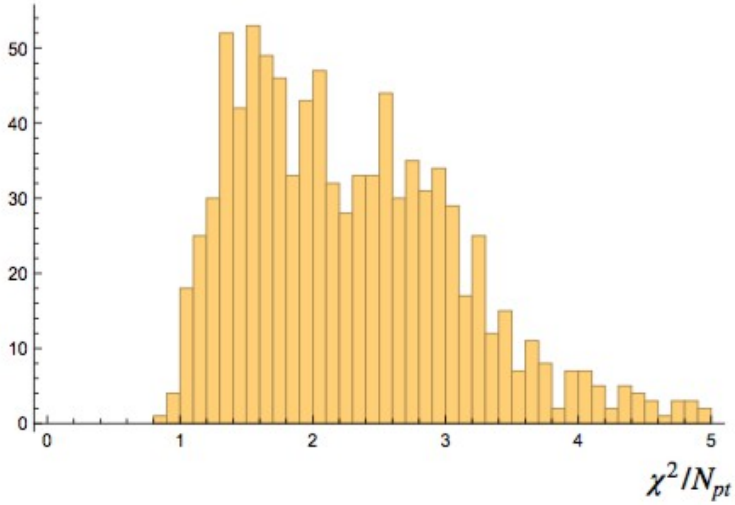

flavor-dependent

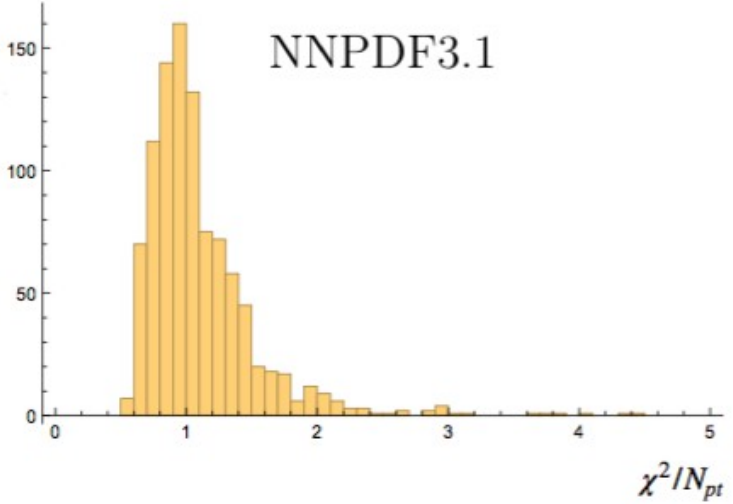

$$f_{NP}(x,b) = \exp\left(-\frac{\lambda_1(1-x)+\lambda_2 x + x(1-x)\lambda_5}{\sqrt{1+\lambda_3 x^{\lambda_4}\mathbf{b^2}}}\mathbf{b^2}\right)$$

$$f^f_{NP}(x,b) = \exp\left(-\frac{\lambda^f_1(1-x)+\lambda^f_2 x}{\sqrt{1+\lambda_0 x^2\mathbf{b^2}}}\mathbf{b^2}\right)$$

$f = u, \bar{u}, d, \bar{d}, sea$

- The figure above is obtained with the NNPDF3.1 set. We have verified that similar features hold for all PDF sets.

- *slide by P. Zurita*

Extracted TMD distributions with inclusion of PDF uncertainty and flavor dependence

Bury et al., JHEP 10 (2022) 118 [arXiv:2201.07114]

- Differences between flavours are clear:
  - **Red** : EXP
  - **Blue** : PDF
  - **Black**: combined

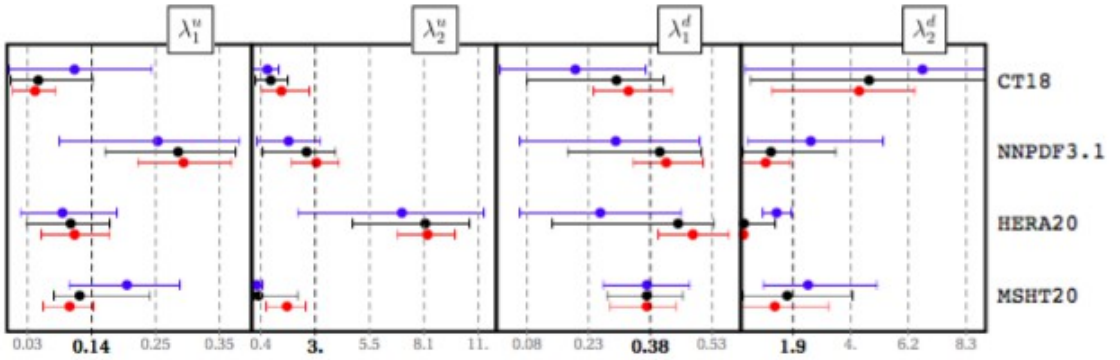

- We obtain realistic uncertainty bands for the TMDPDFs:

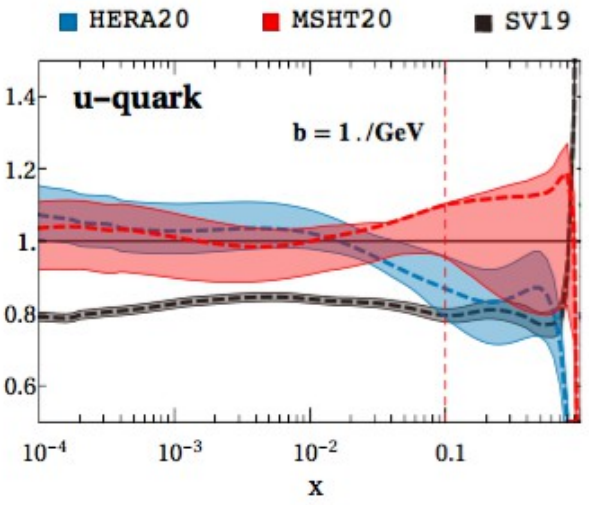

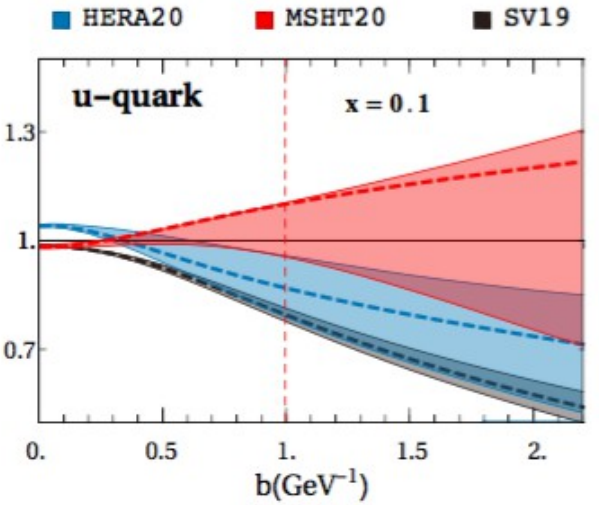

slide by P. Zurita

PDF replicas and qT shapes

- Does varying PDF replicas mostly result into a change in normalization of predictions for qT spectra?
  Not really: different PDF replicas induce different qT shapes.

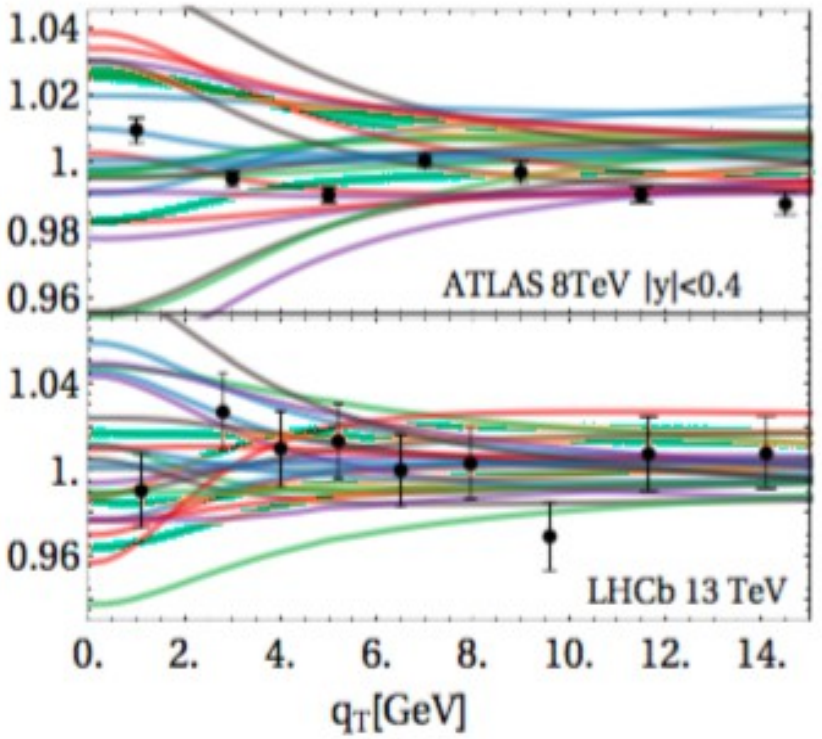

Figure 14: Examples of prediction using different PDF replicas at the same $f_{\rm NP}$.

- This is at the origin of the chi-squared values spread among replicas observed earlier. It is due to the fact that the OPE relation couples the *b* and *x* dependences.

Remarks

Bury et al., JHEP 10 (2022) 118 [arXiv:2201.07114]

- Bayesian analysis to propagate PDF uncertainties to unpolarized TMDs: PDF uncertainties found to be larger than EXP uncertainties for all *b*.

- As a result of the improved analysis framework, TMD error bands are understood to be underestimated in earlier fits based on OPE.

- This also impacts polarized TMD analyses, for which unpolarized cross sections are used to normalize angular distributions and asymmetries.

- Flavor dependence of NP TMD distributions included for the first time in fits based on TMD evolution: i) it reduces the spread in chi-squared distributions over replicas; ii) leads to more consistent results among different PDF sets.

HOW DOES TMD PHYSICS AFFECT THE ASSOCIATED MULTI-JET FINAL STATES?

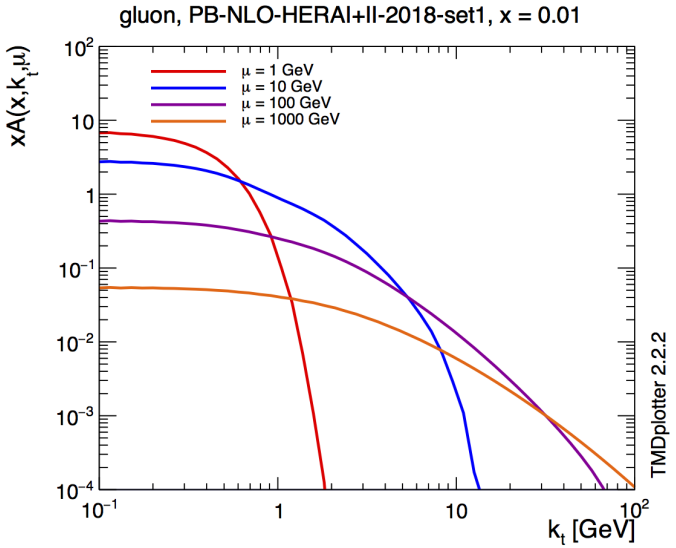

- TMD distribution from fits to eh data
- kT broadening due to initial state radiation
- To assess its impact on the associated jet production, consider the integrated distribution above the jet pT scale:

$$a_j(x, \boldsymbol{k}, \mu^2) = \int \frac{d^2\boldsymbol{k}'}{\pi} \mathcal{A}_j(x, \boldsymbol{k}', \mu^2)\, \Theta(\boldsymbol{k}'^2 - \boldsymbol{k}^2)$$

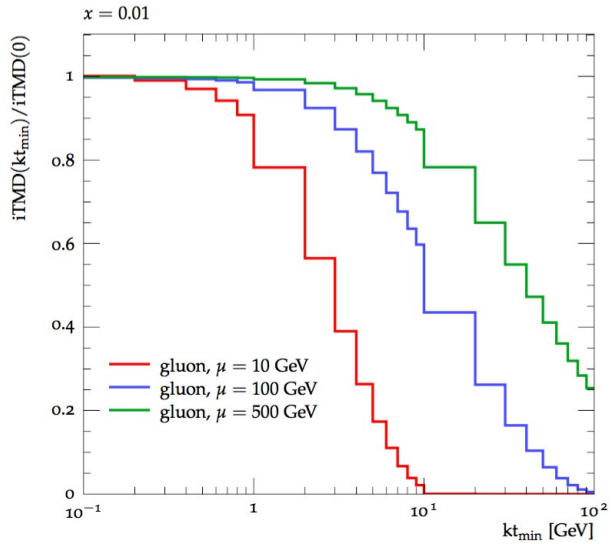

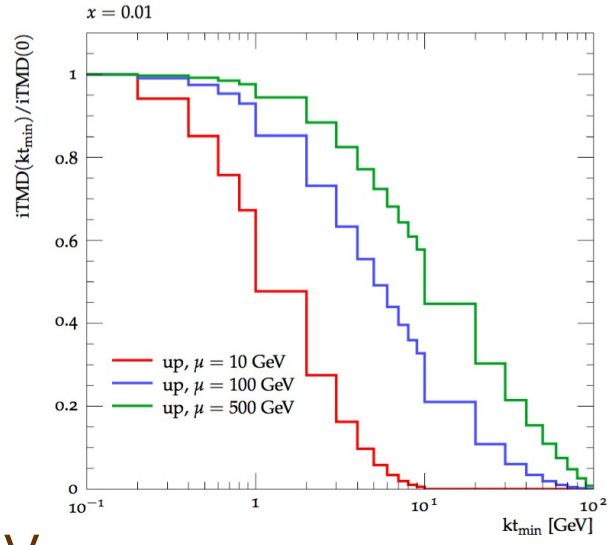

- For instance, for mu = 100 (500) GeV, 30% probability that the gluon has developed kT larger than 20 (80) GeV

STRATEGY

- Adopt parton branching formulation of TMD evolution
- Develop an appropriate jet merging method to include consistently higher multiplicity matrix elements along with TMD evolution
- Explore the influence of transverse momentum recoils and soft radiation on theoretical systematic uncertainties in multi-jet studies
- Key idea: better modeling of emissions of jets that are soft or close to another hard jet can improve multi-jet theoretical systematics

Parton Branching (PB) formulation of TMD evolution

[slide by M. van Kampen]

JHEP 01 (2018) 070 [arXiv:1708.03279]

PB evolution equation for TMDs $\tilde{\mathcal{A}}_a(x, k_t^2, \mu^2)$ can be solved iteratively with the Monte Carlo method:

$$\tilde{\mathcal{A}}_a(x, k_t^2, \mu^2) = \Delta_a(\mu^2, \mu_0^2)\tilde{\mathcal{A}}_a(x, k_{t,0}^2, \mu_0^2) +$$
$$+ \sum_b \left[\int \frac{d^2\boldsymbol{\mu'}}{\pi\mu'^2} \int_x^{z_M(\mu')} dz \Theta(\mu^2 - \mu'^2)\Theta(\mu'^2 - \mu_0^2) \right.$$
$$\left. \times \frac{\Delta_a(\mu^2, \mu_0^2)}{\Delta_a(\mu'^2, \mu_0^2)} P_{ab}^{(R)}(\alpha_s(q_t), z)\tilde{\mathcal{A}}_b\left(\frac{x}{z}, \underbrace{k_{t,b} - q_{t,c}}_{k_{t,a}}, \mu'^2\right) \right]$$

Kinematics in each branching governed by momentum conservation: $k_{t,b} = k_{t,a} + q_{t,c}$

$P_{ab}^{(R)}(\alpha_s, z)$ real splitting function (resolvable branching probability),
$\Delta_a(\mu^2, \mu_0^2)$ Sudakov (no branching probability)

Angular ordering condition: $q_t^2 = (1-z)^2\mu'^2$

$$P_{ab}^{(R)}(\alpha_s, z) = \sum_{n=1}^{\infty} \left(\frac{\alpha_s}{2\pi}\right)^n P_{ab}^{(R)n-1}(z)$$

$$\Delta_a(\mu^2, \mu_0^2) = \exp\left(-\sum_b \int \frac{d\mu^2}{\mu^2} \int_0^{z_M} dz\, z\, P_{ab}^{(R)}(z, \alpha_s)\right)$$

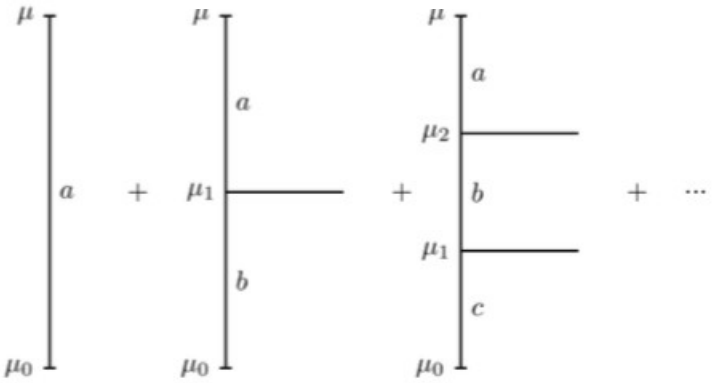

Parton Branching (PB) formulation of TMD evolution

[slide by M. van Kampen]

Analytical comparison CSS and PB: logarithmic accuracy

CSS Sudakov (with scale $\mu = q_t$):

$$S(Q^2, b^2) = \exp\left(-\int_{1/b^2}^{Q^2} \frac{dq_t^2}{q_t^2}\left[\ln\left(\frac{Q^2}{q_t^2}\right) A_a(\alpha_s(q_t^2)) + B_a(\alpha_s(q_t^2))\right]\right)$$

PB Sudakov (*twice in the cross section!*) rewritten with angular ordering and virtual splitting functions:

$$\Delta_a^{(PB)}(Q^2, q_0^2) = \exp\left(-\int_{q_0^2}^{Q^2} \frac{dq_t^2}{q_t^2}\left[\frac{1}{2}\ln\left(\frac{Q^2}{q_t^2}\right) k_a(\alpha_s(q_t^2)) - d_a(\alpha_s(q_t^2))\right]\right)$$

Logarithmic accuracy	Terms	Single log	Double log	
Leading log (LL)	$\alpha_s^n \ln^{n+1}(Q^2/q_t^2)$		$A_a^{(1)} = 1/2 k_a^{(0)}$	✓
Next-to-leading log (NLL)	$\alpha_s^n \ln^{n}(Q^2/q_t^2)$	$B_a^{(1)} = -d_a^{(0)}$	$A_a^{(2)} = 1/4 k_a^{(1)}$	✓
Next-to-next-to-leading log (NNLL)	$\alpha_s^n \ln^{n-1}(Q^2/q_t^2)$	$B_q^{(2)} = -1/2 d_q^{(1)}$ $+4\pi C_F \beta_0 (\zeta_2 - 1)$ ⇓ *Resummation scheme dependence*	$A_q^{(3)} = 1/8 k_q^{(2)}$ $+2\beta_0 C_F d_2^{q\,*}$ ⇓ *Effective α_s*	✓/✗

Soft-gluon effective coupling: Banfi et al. [arXiv:1807.11487] & Catani et al. [arXiv:1904.10365]

$$^*d_2^q = C_F C_A \left(\frac{808}{27} - 28\zeta_3\right) - \frac{112}{27} C_F N_f$$

Mees van Kampen (Uni. Antwerp) | Comparison PB and analytical resummation | DIS 2021 | 6 / 11

3D Imaging and Monte Carlo

Backward evolution with PB method

The TMD evolution equation can be used to do a backward evolution:

$$\frac{\partial}{\partial \ln \mu^2}\left(\frac{\tilde{\mathcal{A}}_a(x,k_t,\mu)}{\Delta_a(\mu)}\right) = \sum_b \int_x^{z_M} dz P_{ab}^{(R)} \frac{\tilde{\mathcal{A}}_b(x/z,k_t',\mu)}{\Delta_a(\mu)},$$

normalize to $\frac{\tilde{\mathcal{A}}_a(x,k_t,\mu)}{\Delta_a(\mu)}$ and integrate over μ' from μ_i down to μ_{i-1}

$$\Delta_{bw}(x,k_t,\mu_i,\mu_{i-1}) = \exp\left\{-\sum_b \int_{\mu_{i-1}^2}^{\mu_i^2} \frac{d\mu'^2}{\mu'^2} \int_x^{z_M} dz P_{ab}^{(R)} \frac{\tilde{\mathcal{A}}_b(x/z,k_t',\mu')}{\tilde{\mathcal{A}}_a(x,k_t,\mu')}\right\}.$$

This Sudakov is used as the no-branching probability in the TMD parton shower.

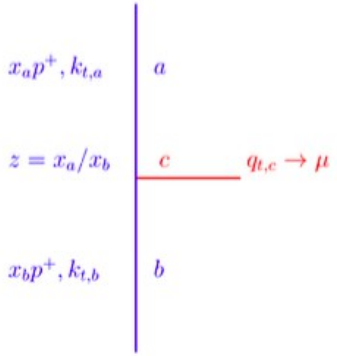

- In each splitting

$$\begin{aligned} \boldsymbol{k}_{t,b} &= \boldsymbol{k}_{t,a} + \boldsymbol{q}_{t,c} \\ &= \boldsymbol{k}_{t,a} + (1-z)\mu \end{aligned}$$

- Total transverse momentum:

$$\boldsymbol{k}_t = \boldsymbol{k}_{t,0} + \sum_c q_{t,c}$$

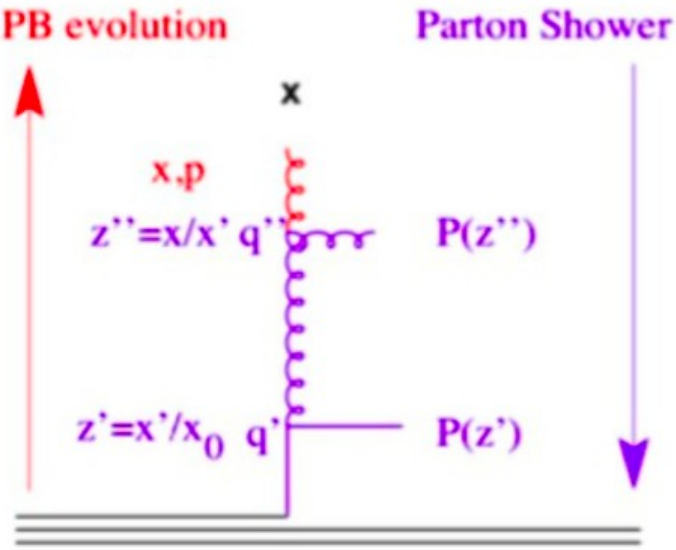

• implementation in the Cascade Monte Carlo: *arXiv:2101.10221*

Z-boson Drell-Yan production at the LHC by PB-TMD (TMDs fitted to inclusive DIS) x (NLO DY calculation)

A Bermudez et al, PRD 100 (2019) 074027 [arXiv:1906.00919]

- Use MadGraph5_aMC-at-NLO
- Apply PB-TMD
- Set matching scale mu_m (kT < mu_m)

ATLAS 8 TeV data [E. Phys. J. C76 (2016) 291]

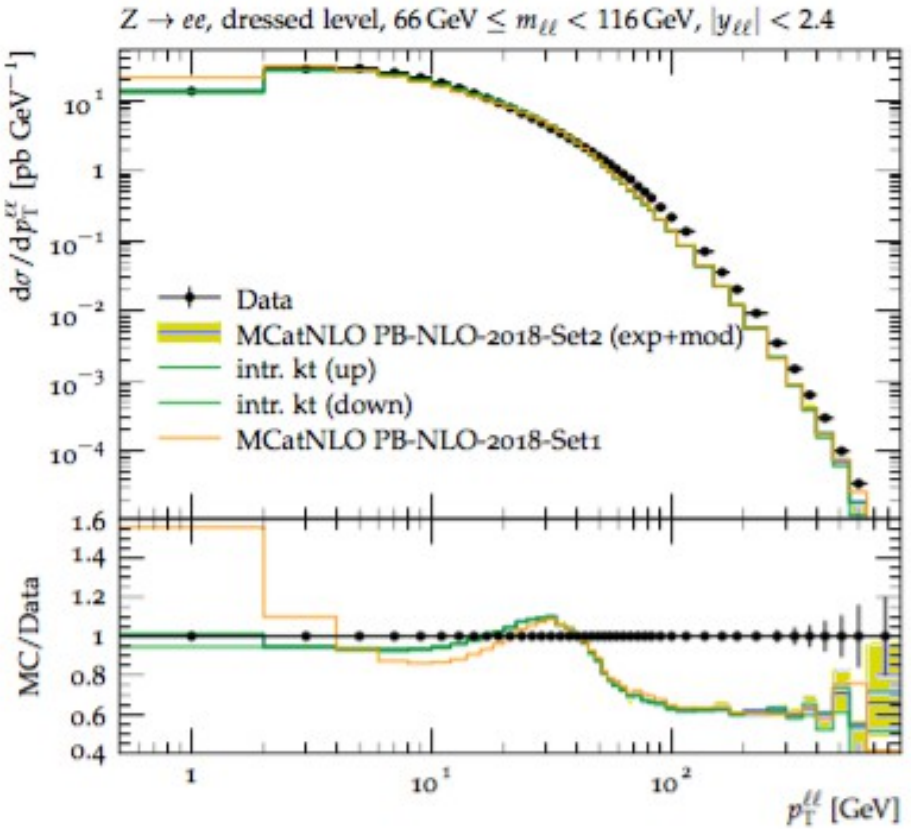

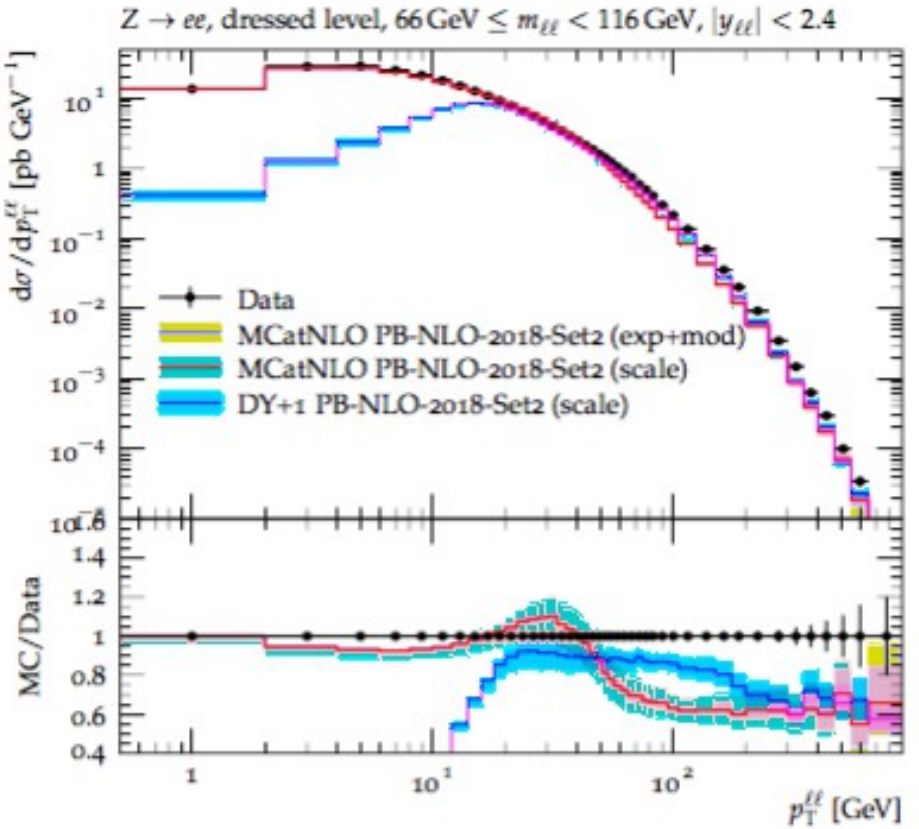

- Theoretical uncertainties dominated by scale dependences; TMD uncertainties moderate
- Low-pT spectrum sensitive to angular ordering (PB-TMD Set 2)
- Missing higher orders at high pT: DY + jet contribution (blue curve on right hand side)

TMD multi-jet merging method

[Bermudez Martinez, Mangano & H, Phys. Lett. B 822 (2021) 136700; arXiv:2208.02276]

- Evaluate the ME for n-jet cross sections
- Reweight the strong coupling according to shower history
- **Evolve the ME using the TMD PB evolution**
- **Shower the events using the backward PB evolution for ISR**
- **Apply the MLM(*) prescription between the PB-evolved ME and the showered events**

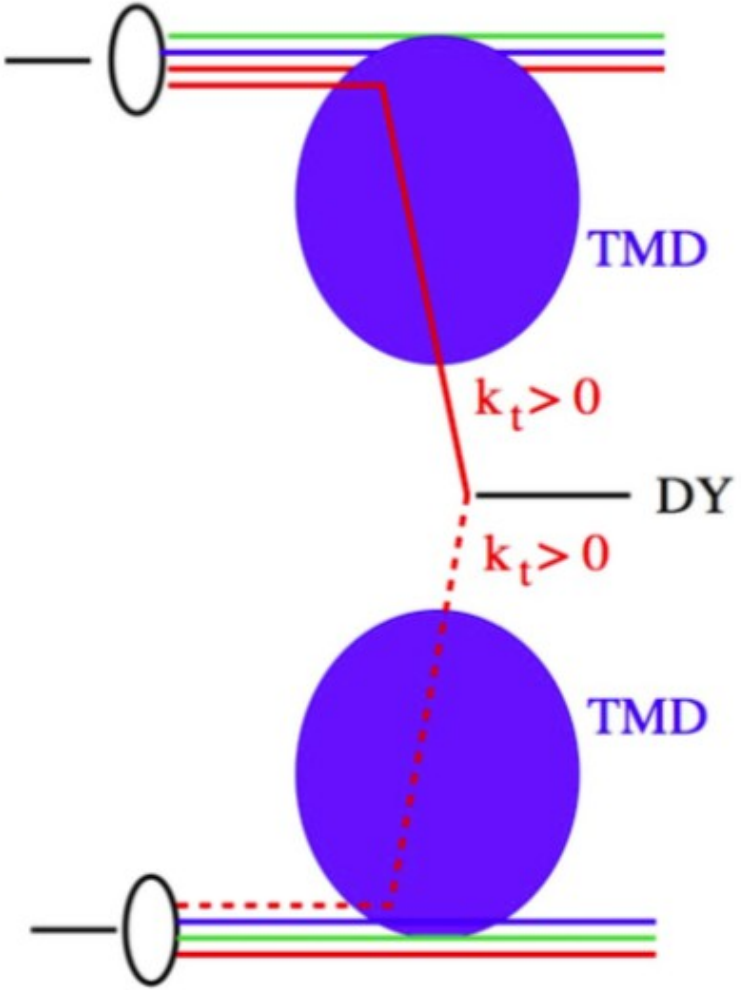

New merging procedure applicable to TMDs!

* The method can be used with other prescriptions as well, such as CKKW-L. We here focus on MLM in presenting explicit results.

Z-BOSON TRANSVERSE MOMENTUM

[Bermudez Martinez, Mangano & H , PLB 822 (2021) 136700 [arXiv:2107.01224]]

- *TMD-merged result*
- *compared with result without TMD merging*

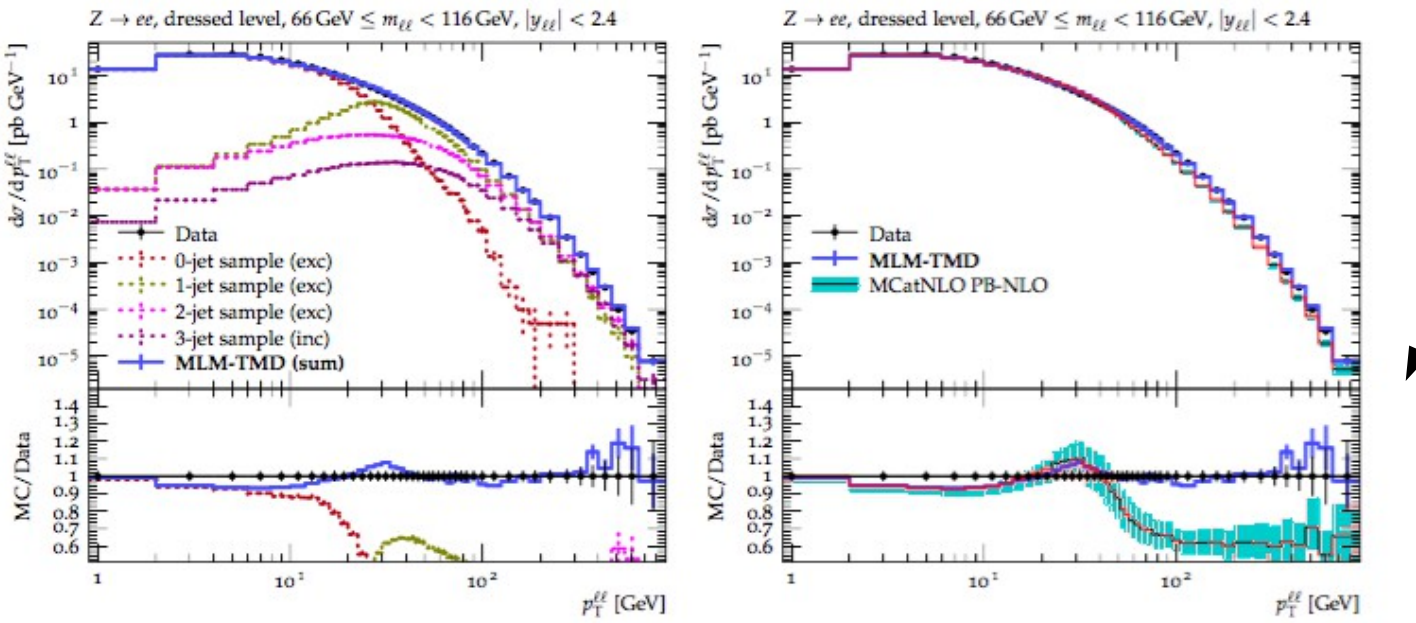

FIG. 3: Transverse momentum p_T spectrum of Z-bosons DY lepton pairs from Z-boson decays. Experimental measurements by ATLAS [39] at $\sqrt{s} = 8$ TeV are shown. Left: result of the MLM-TMD calculation and separate contributions from the different jet samples. All jet multiplicities are obtained in exclusive (exc) mode except for the highest multiplicity which is calculated in inclusive (inc) mode. Right: the curves show the MLM-TMD calculation and the NLO calculation of Ref. [29], based on inclusive Z production. The uncertainty band on the NLO calculation represents the TMD and scale uncertainties as discussed in [29].

Phi-star distribution of DY lepton pairs by TMD multi-jet merging

[Bermudez Martinez, Mangano & H , JHEP 09 (2022) 060 [arXiv:2208.02276]]

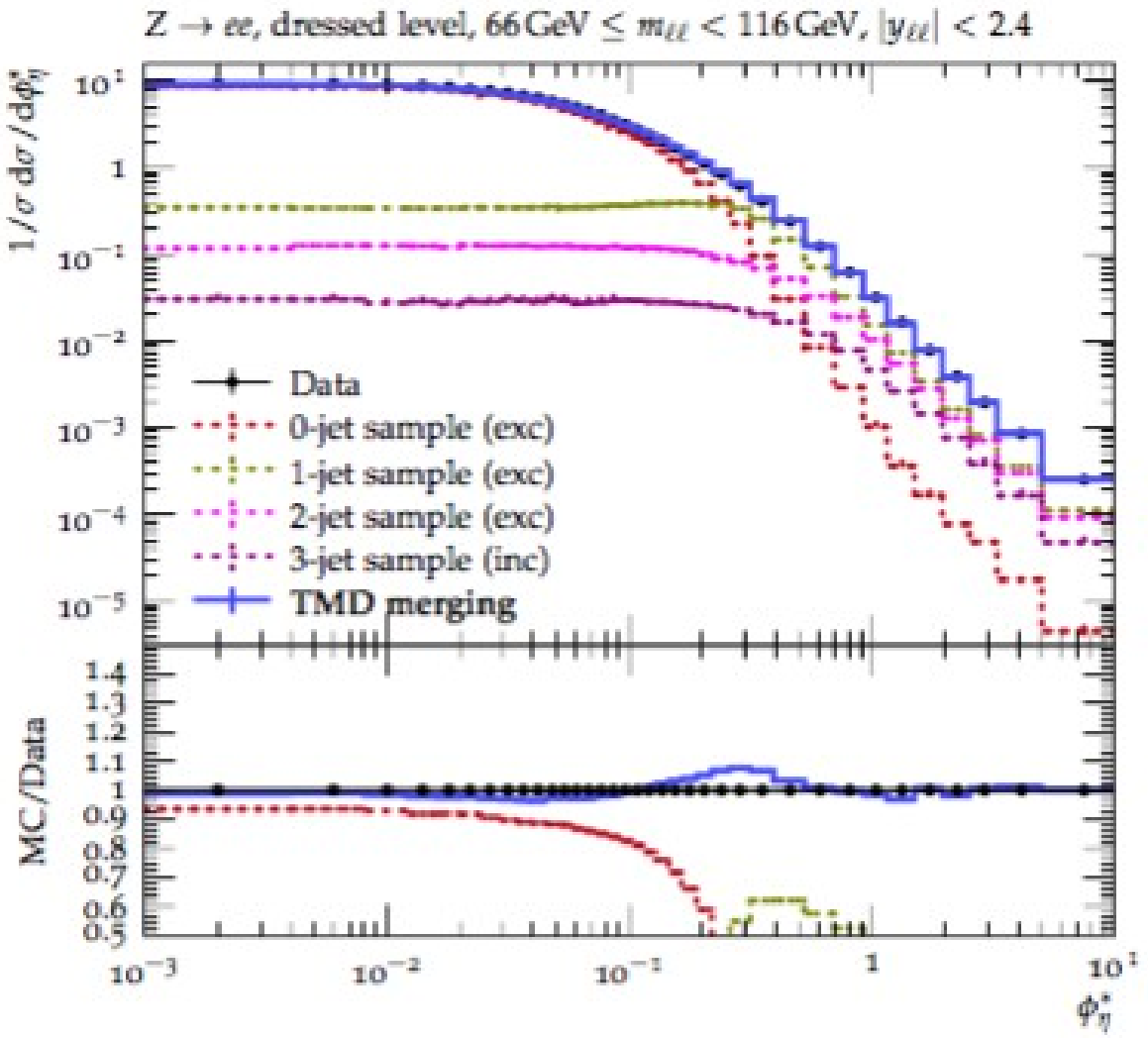

ATLAS 8 TeV data

JET MULTIPLICITIES IN Z+JETS

- Not only the overall DY recoil but also the number of jets are described by TMD merging
- This holds up to multiplicities much larger than the number of jets (three) for which ME is calculated, owing to TMD evolution describing better non-collinear emissions.

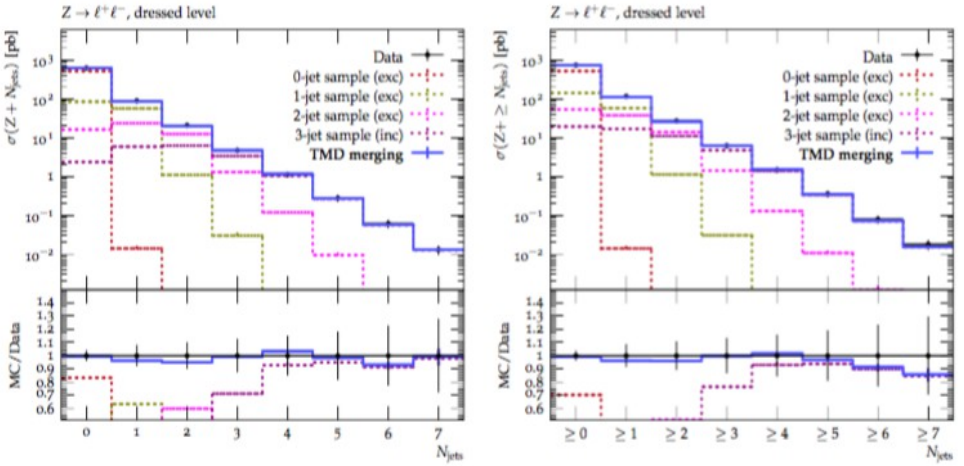

Figure 10. Exclusive (left) and inclusive (right) jet multiplicity distributions in the production of a Z-boson in association with jets. Experimental measurements by ATLAS [91] at $\sqrt{s} = 13$ TeV are compared to predictions using the TMD merging calculation. Separate contributions from the different jet samples are shown. All the jet multiplicities are obtained in exclusive (exc) mode except for the highest multiplicity which is calculated in inclusive (inc) mode.

TMD merging vs. collinear merging comparison

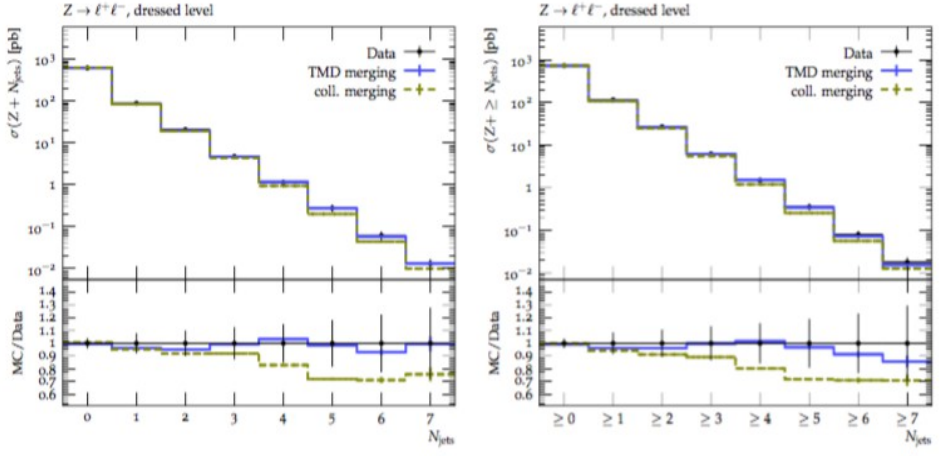

Figure 23. Predictions obtained using MADGRAPH+PYTHIA6 with MLM merging and the TMD merging framework are compared for exclusive (left) and inclusive (right) jet multiplicity distributions in the production of a Z-boson in association with jets, at $\sqrt{s} = 13$ TeV. The phase space for the calculation follows the one in [91], whose data are included in these and subsequent plots.

Bermudez Martinez, Mangano & H, JHEP 09 (2022) 060 [arXiv:2208.02276]

ASSOCIATED JET pT SPECTRA IN Z + JETS

Bermudez Martinez, Mangano & H, JHEP 09 (2022) 060 [arXiv:2208.02276]

- The description of jet transverse momentum improves thanks to TMD merging with respect to collinear merging at high multiplicities

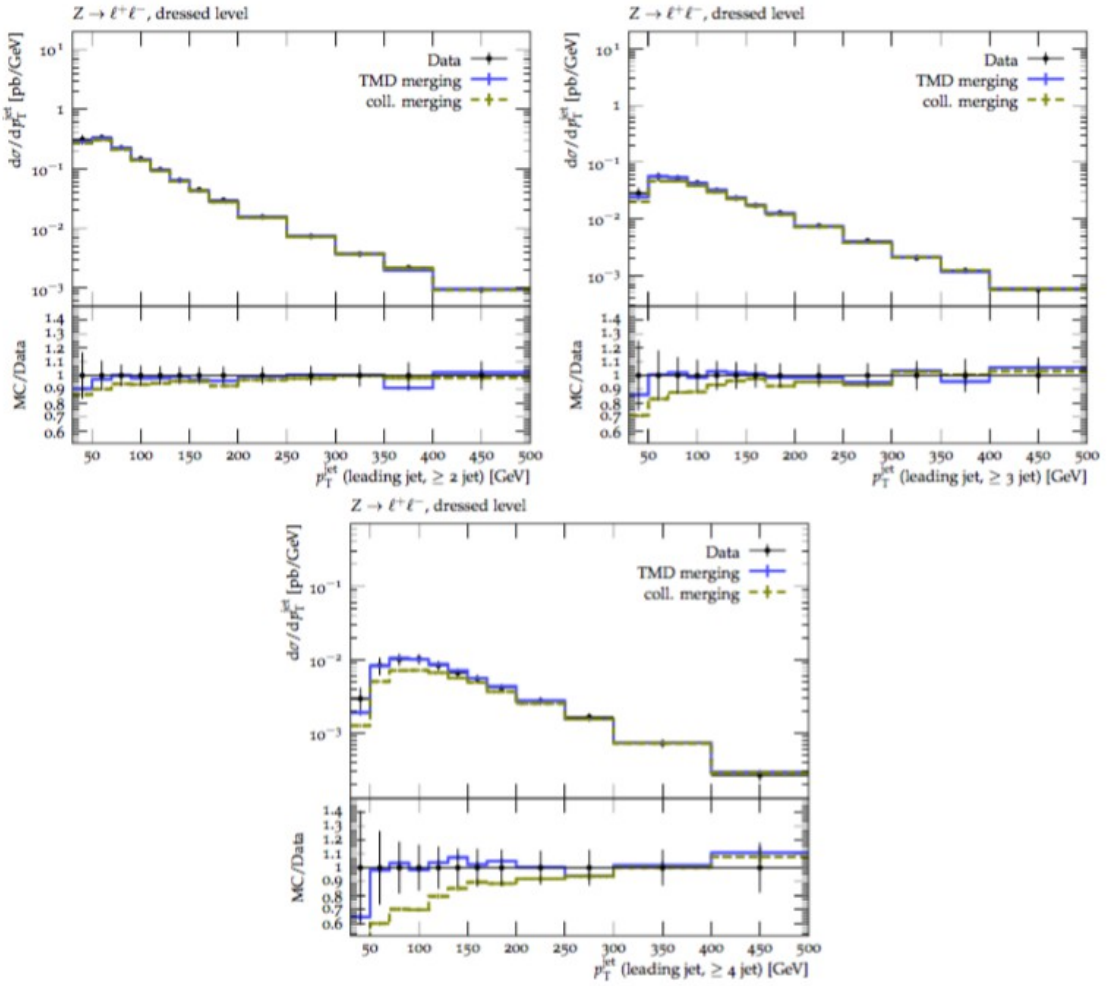

Figure 25. Predictions obtained using MADGRAPH+PYTHIA6 with MLM merging, and the TMD merging framework are compared for the leading jet p_T spectrum in inclusive Z+2 (top left), 3 (top right), and 4 (bottom) jets. The phase space for the calculation follows the one in [91].

DI-JET AZIMUTHAL SEPARATION IN Z+JETS

Bermudez Martinez, Mangano & H, JHEP 09 (2022) 060 [arXiv:2208.02276]

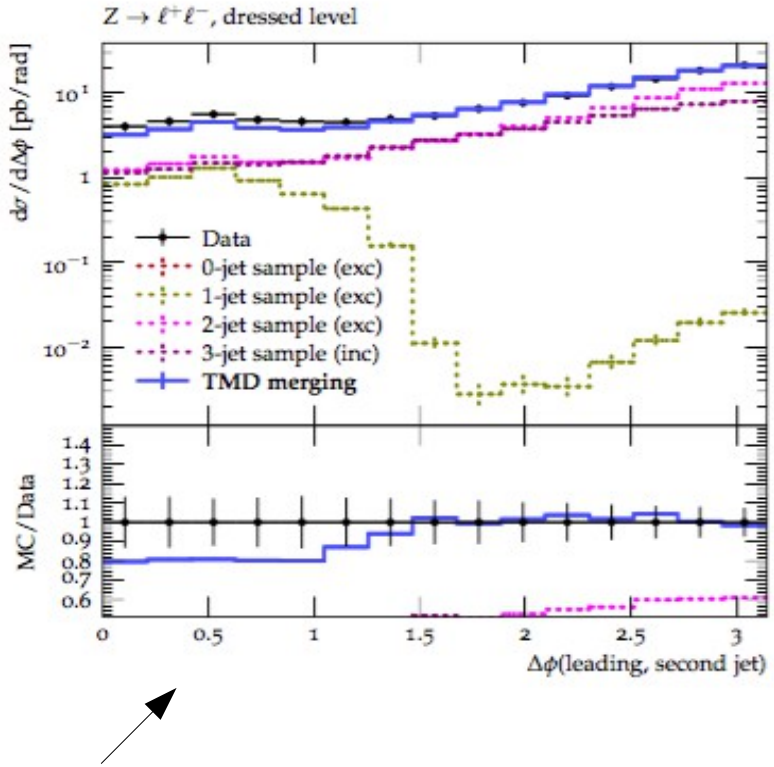

20% deficit at low Delta-phi
(single-parton interaction)

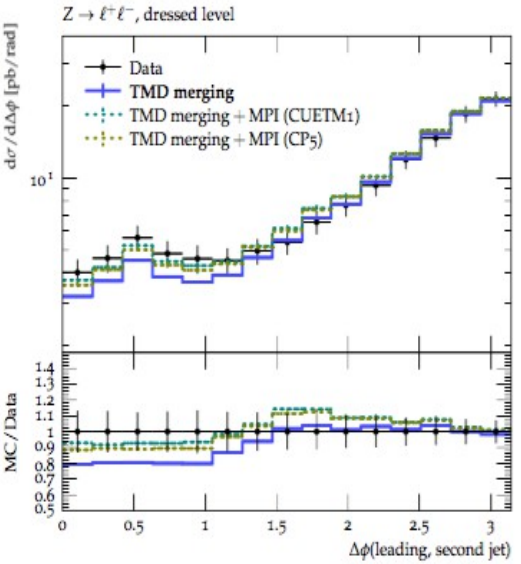

Figure 14. Di-jet azimuthal separation distribution for $Z+\geq 2$ jets events. Experimental measurements by ATLAS [74] at $\sqrt{s} = 13$ TeV are compared to predictions using the TMD merging calculation. The results including the MPI correction, estimated using the PYTHIA8 tunes CUETP8M1 [83] and CP5 [84], are shown with dashed lines.

- Multi-parton interaction (MPI) interpretation:
  Z+1 jet primary interaction
  with 2-jet second interaction.
- Estimate by P8 MPI models.

Theoretical systematics: dependence of multi-jet cross sections on the merging scale

Merging scale [GeV]	σ[tot] [pb]	σ[≥ 1 jet] [pb]	σ[≥ 2 jet] [pb]	σ[≥ 3 jet] [pb]	σ[≥ 4 jet] [pb]
23	1145.95	174.51	40.53	9.67	2.36
33	1126.07	172.30	40.95	9.72	2.38

- 10 GeV variation gives **< 2% change** in jets cross sections
- Standard merging algorithms can give over 10 % change for the same variation of the merging scale CF: J. Alwall et al. [EPJC 53, 473–500 (2008)]

→ Dependence on merging scale reduced by treating transverse momentum in the initial state

Theoretical systematics: dependence on the merging scale

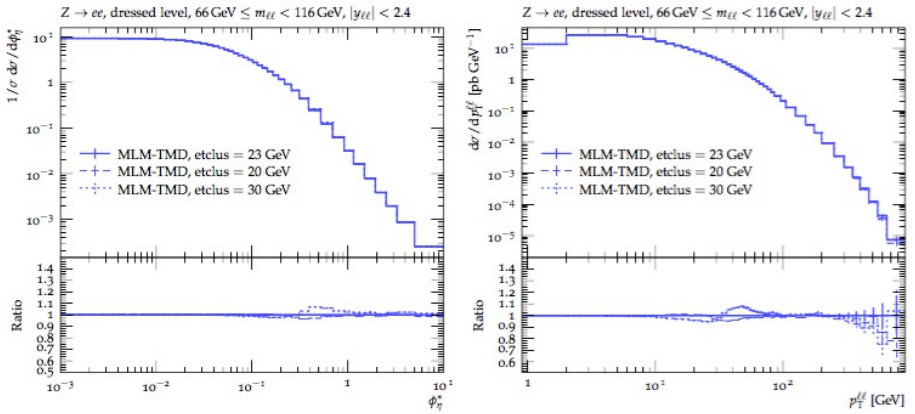

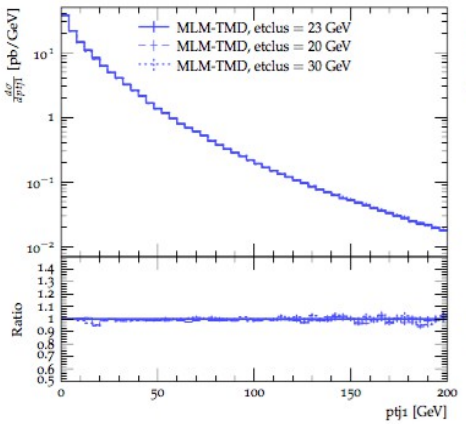

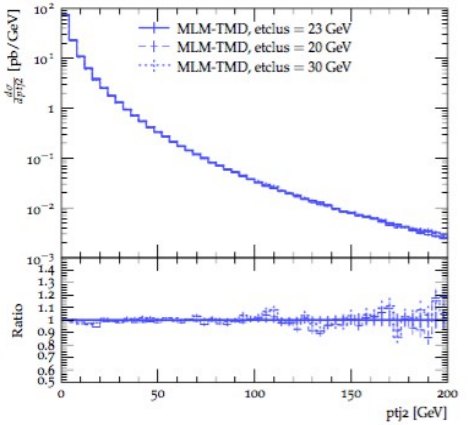

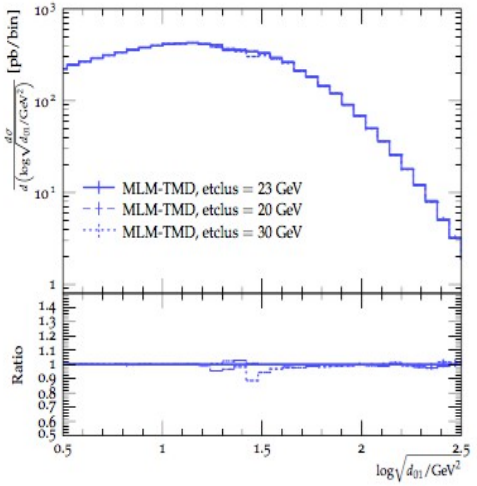

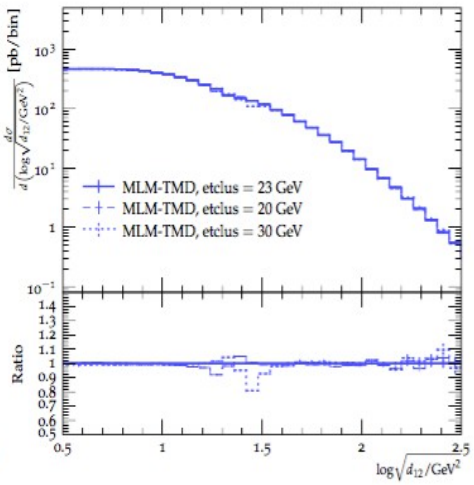

- Effect of variations is localized around the merging scale
- Reduced by inclusion of transverse momenta in the initial state

Outlook

- TMD methodology relevant to both low-pT and high-pT collider processes
- Consistent physical picture of Drell-Yan transverse momentum spectra, from LHC to fixed-target energies (and DIS precision measurements)
- Implications on structure of jet final states have just begun to be explored
- TMD multi-jet merging techniques extendable to NLO merging and alternative matching algorithms

FUTURE DEVELOPMENTS: CAN THIS BE EXTENDED TO COLORFUL PROCESSES?

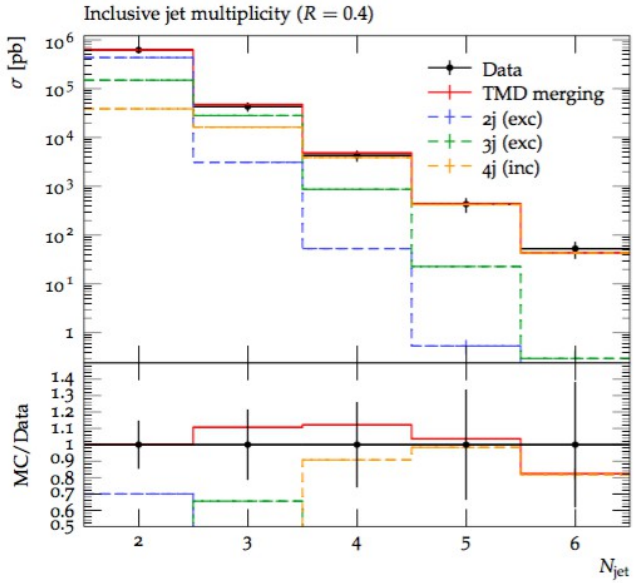

- *preliminary – application to ATLAS 7 TeV multi-jets*

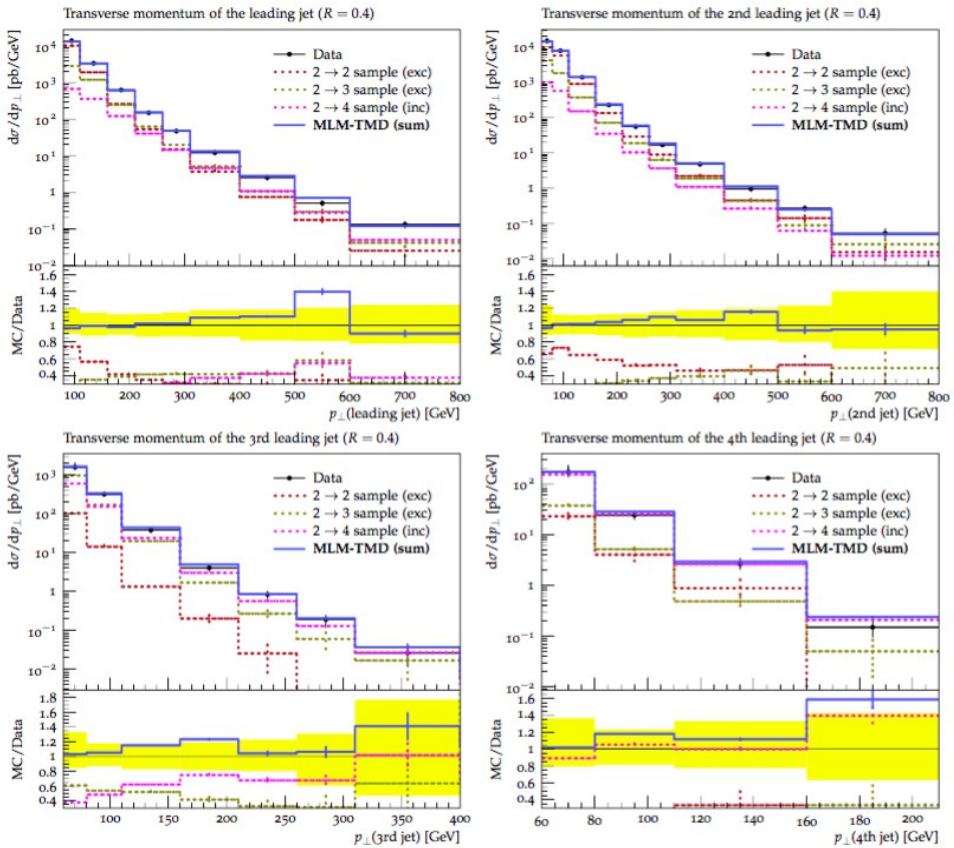

- NB: theoretical systematics of merging in pure-jet case yet to be explored even in collinear setting
- Jet correlation measurements to probe QCD multi-scale dynamics
- Potentially relevant for b b-bar and t t-bar final states

Bermudez Martinez, Mangano, van Kampen & H, in progress

APPLICATION TO SOFT PRODUCTION - WHAT IS THE IMPACT ON UNDERLYING EVENTS?

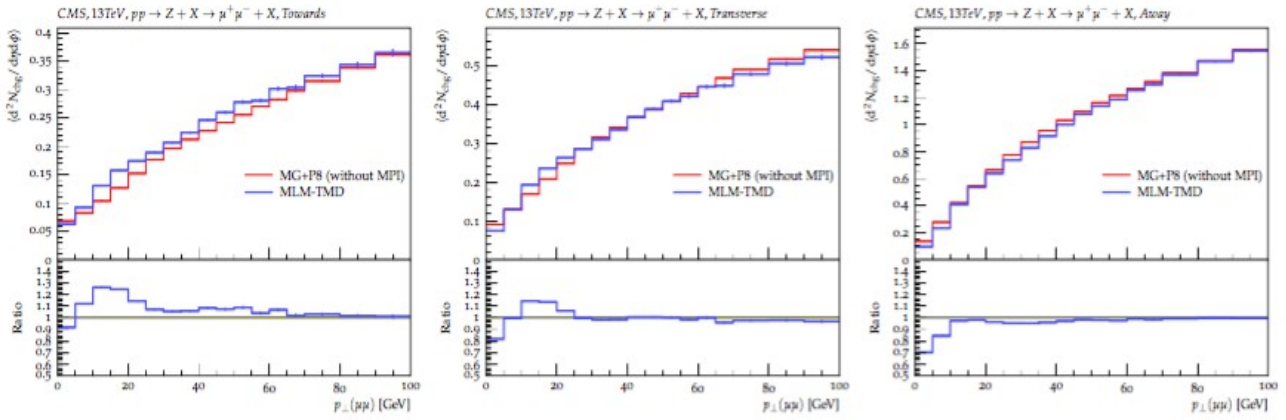

Figure 3: *Comparison of parton-showering contributions, Pythia8 versus MLM-TMD, to underlying events: charged particle multiplicity in the (left) towards, (middle) transverse and (right) away regions.*

- *preliminary – application to CMS underlying events in Z production at 13 TeV*

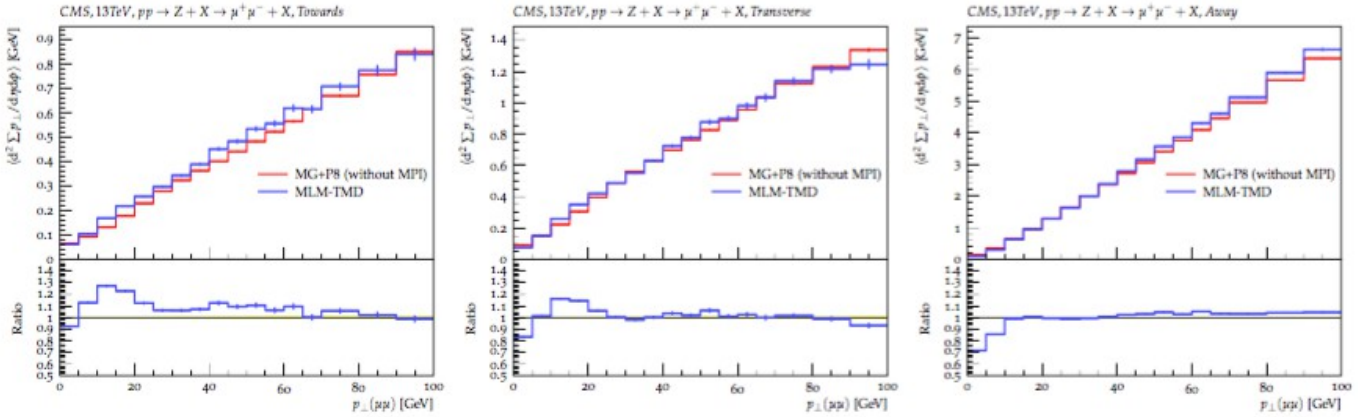

Figure 4: *Comparison of parton-showering contributions, Pythia8 versus MLM-TMD, to underlying events: sum of charged particle transverse momenta in the (left) towards, (middle) transverse and (right) away regions.*

- *MPI contribution to UE subtracted*
- *Showering contribution to charged particle multiplicity and transverse momenta affected by TMD shower for low muon pair pT*

Conclusion

- Precision SM physics and new physics searches at shortest distances and highest mass depend on chromodynamic effects which probe the structure of the theory beyond finite-order perturbation expansions.

- Advances in theoretical methods of factorization and resummation are essential to fully exploit the potential of experimental measurements, and will affect both the intensity frontier with the LHC upgrade phase and the energy frontier of future colliders.

EXTRA SLIDES

“The TMDlib project” http://tmdlib.hepforge.org/

- a platform for theory and phenomenology of TMD pdfs
- library of fits and parameterizations LHApdf style

DESY 14-059
NIKHEF 2014-024
RAL-P-2014-009
YITP-SB-14-24
Dec 2014

TMDlib and TMDplotter: library and plotting tools for transverse-momentum-dependent parton distributions

F. Hautmann[1,2], H. Jung[3,4], M. Krämer[3], P. J. Mulders[5,6], E. R. Nocera[7], T. C. Rogers[8,9], A. Signori[5,6]

[1] Rutherford Appleton Laboratory, UK
[2] Dept. of Theoretical Physics, University of Oxford, UK
[3] DESY, Hamburg, FRG
[4] University of Antwerp, Belgium
[5] Department of Physics and Astronomy, VU University Amsterdam, the Netherlands
[6] Nikhef, the Netherlands
[7] Università degli Studi di Genova and INFN Genova, Italy
[8] C.N. Yang Institute for Theoretical Physics, Stony Brook University, USA
[9] Department of Physics, Southern Methodist University, Dallas, Texas 75275, USA

Abstract

Transverse-momentum-dependent distributions (TMDs) are extensions of collinear parton distributions and are important in high-energy physics from both theoretical and phenomenological points of view. In this manual we introduce the library TMDlib, a tool to collect transverse-momentum-dependent parton distribution functions (TMD PDFs) and fragmentation functions (TMD FFs) together with an online plotting tool, TMDplotter. We provide a description of the program components and of the different physical frameworks the user can access via the available parameterisations.

Eur. Phys. J. C (2021) 81:752
https://doi.org/10.1140/epjc/s10052-021-09508-8

THE EUROPEAN PHYSICAL JOURNAL C

Special Article - Tools for Experiment and Theory

TMDlib2 and TMDplotter: a platform for 3D hadron structure studies

N. A. Abdulov[1], A. Bacchetta[2], S. Baranov[3], A. Bermudez Martinez[4,a], V. Bertone[5], C. Bissolotti[2,6], V. Candelise[7,8], L. I. Estevez Banos[4], M. Bury[9], P. L. S. Connor[4,21], L. Favart[10], F. Guzman[11], F. Hautmann[12,13], M. Hentschinski[14], H. Jung[4,b], L. Keersmaekers[12], A. Kotikov[15], A. Kusina[16], K. Kutak[16], A. Lelek[12], J. Lidrych[4], A. Lipatov[1], G. Lykasov[15], M. Malyshev[1], M. Mendizabal[4], S. Prestel[17], S. Sadeghi Barzani[12,18], S. Sapeta[16], M. Schmitz[4], A. Signori[2,19], G. Sorrentino[7,8], S. Taheri Monfared[4], A. van Hameren[16], A. M. van Kampen[12], M. Vanden Bemden[10], A. Vladimirov[9], Q. Wang[4,20], H. Yang[4,20]

A purely factorization-based approach to TMD extraction

Factorization formula of schematic form (up to power corrections):

$$\frac{d\sigma}{dq_T^2} = \sum_{i,j} \int d^2b\, e^{ib\cdot q_T}\, \sigma_{ij}^{(0)}\, f_{1,i\leftarrow h1}(x_1, b; \mu, \zeta_1)\, f_{1,j\leftarrow h2}(x_2, b; \mu, \zeta_2)$$

+ appropriate evolution equations for the TMD distributions *f*

- Measure observable on left hand side; extract *f* on right hand side
- *f* nonperturbative quantity, determined with experimental uncertainties (due to data) and theoretical uncertainties (due to factorization and evolution)

- This would be in the spirit of
  Jung, Mulders, Kraemer, Nocera, Rogers, Signori & H,
  "TMDlib", Eur. J. Phys. C 74 (2014) 3220 [arXiv:1408.3015]

Extraction of TMD distributions using OPE relations

- OPE: *f* is expanded along collinear PDFs, with *b^2* power corrections

$$f_{1,f\leftarrow h}(x,b;\mu,\zeta)=\sum_{f'}\int_x^1\frac{dy}{y}C_{f\leftarrow f'}(y,b;\mu,\zeta)\,q_{f'}\left(\frac{x}{y},\mu\right)+O(b^2)$$

- Ansatz is made for the large-*b*, nonperturbative *f_NP*

$$f_{1,f\leftarrow h}(x,b;\mu,\zeta)=\sum_{f'}\int_x^1\frac{dy}{y}C_{f\leftarrow f'}(y,b;\mu,\zeta)\,q_{f'}\left(\frac{x}{y},\mu\right)f^f_{\rm NP}(x,b)$$

and *f_NP* is fitted.

- “PDF bias” (an *f_NP* for every PDF set or PDF replica)

- fits so far include flavor dependence in PDF but not in *f_NP*

- We address these two issues next.

STRATEGY – Part I

[Bury et al., JHEP 10 (2022) 118]

- Take PDF sets HERA2.0, NNPDF3.1, CT18 and MSHT20, representative of different methodological approaches at NNLO
- Perform fits to unpolarized DY production at small qT, from fixed-target to LHC energies
- Use a Bayesian procedure to propagate PDF uncertainties, for each PDF set, to TMD extractions
- Obtain results for the fitted NP TMD distributions which display, for the first time, both experimental and PDF uncertainties.

STRATEGY – Part II

[Bury et al., JHEP 10 (2022) 118]

- Go beyond the assumption of flavor-independent *f_NP* used so far in the literature, and include flavor dependence in NP TMD distributions.

  To this end we will use the parameterization

$$f_{\mathrm{NP}}^{f} = \exp\left(-\frac{(1-x)\lambda_1^f + x\lambda_2^f}{\sqrt{1+\lambda_0 x^2 b^2}} b^2\right)$$

- Assess the impact of flavor dependence on fits: study the distribution of chi-squared values over PDF replicas, for each PDF set, in the flavor-dependent case compared to the flavor-independent case; examine the consistency of results across different collinear PDF sets.

Perturbative Scale Variation

To better appreciate the role of the PDF and EXP uncertainty bands in figs. 3-4, we next consider the theoretical uncertainty bands obtained by variation of the perturbative scales. We perform the scale variation according to the ζ prescription approach in [6, 37]. This amounts to varying two scales, the factorization scale in the DY cross section formula and the small-b matching scale in the OPE expansion of the solution of TMD evolution equations. (The small-b matching scale of the CS-kernel is present in this approach but its variation is not included in the calculation.) We vary these scales by factors c in the range $[0.5, 2]$, and take the maximum symmetrized deviation. The resulting bands are shown in fig. 5.

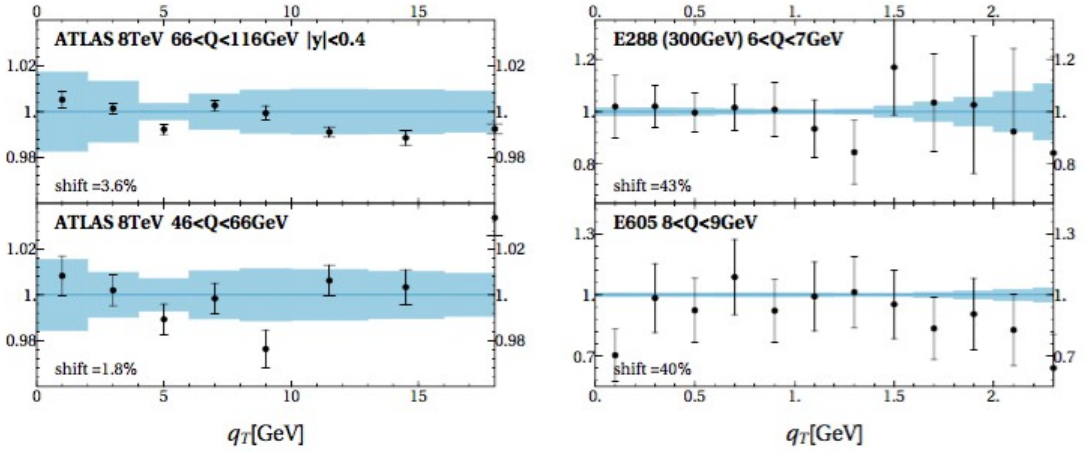

Figure 5: Scale variation band in comparison to typical data at high (left panel) and low (right panel) energies. The scale variation band is defined as the maximum symmetrized deviation from varying all scale parameters by a factor $c \in [0.5, 2]$.

We observe that the PDF uncertainty bands in fig. 3 are comparable or larger than the perturbative scale variation bands in fig. 5. This underlines that DY transverse momentum measurements in the TMD region are potentially useful to place constraints on PDFs. For this purpose one needs to employ a theoretical framework capable of describing the low transverse momentum region. One could envisage doing this in a resummation framework, formulated in terms of collinear PDF only, or in a TMD framework, in which a joined fit of both PDFs and TMDPDFs will put extra constraints on the PDFs.

Bury et al., arXiv:2201.07114

DIFFERENTIAL JET RATES (DJR) IN Z+JETS PRODUCTION

[Bermudez Martinez, Mangano & H, arXiv:2109.08173 (Rencontres La Thuile 2021)]

- smoothness - - > merging follows shower Sudakov suppression

- merging scale divides phase space for different jet multiplicities avoiding double counting or missing events

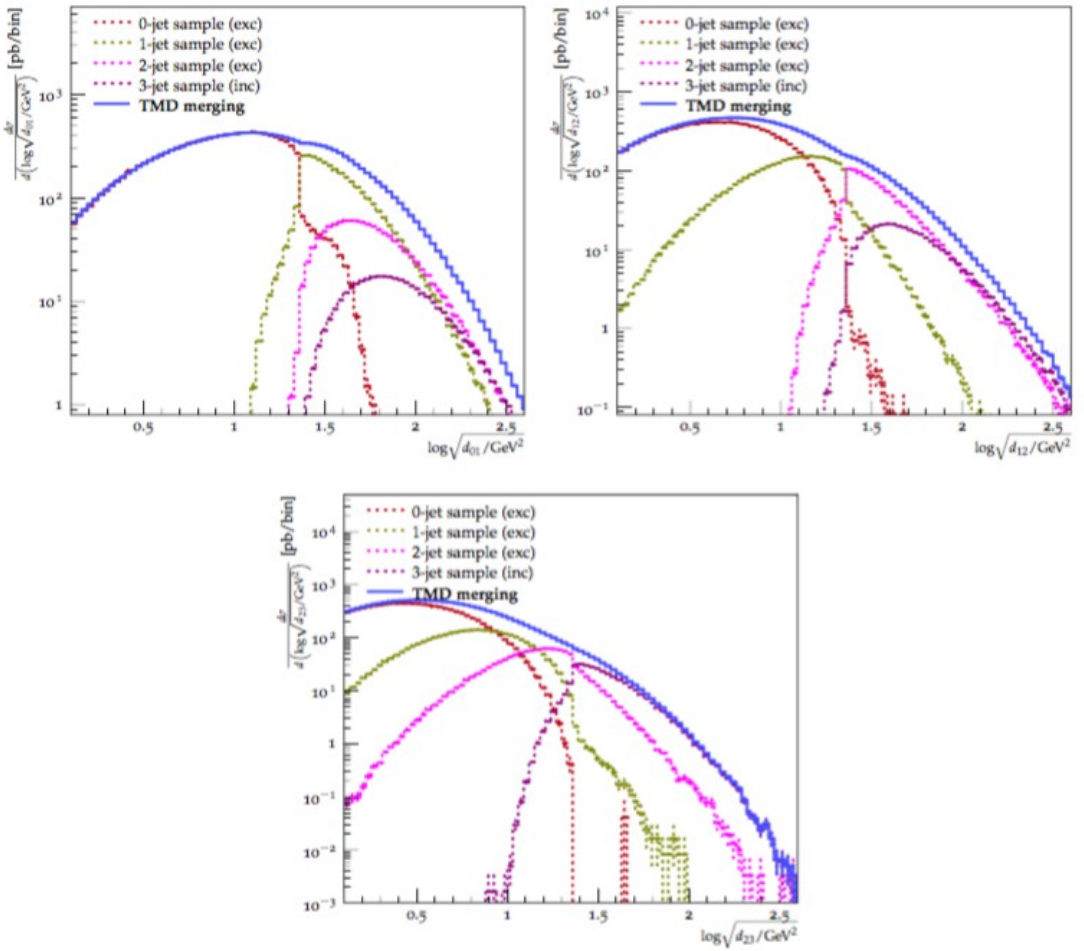

Figure 8. The $d_{n,n+1}$ spectra for $n = 0, 1, 2$ at parton level, where $d_{n,n+1}$ represents the energy-square scale at which an $(n+1)$-jet event is resolved as an n-jet event in the $k_\perp$ jet-clustering algorithm. The dotted curves represent the contributions of the single-multiplicity samples while the solid curve corresponds to their sum. For each panel all jet multiplicities are obtained in exclusive (exc) mode except for the highest multiplicity which is calculated in inclusive (inc) mode.